

Process-Property Relationships of Ti6Al4V Fabricated through Selective Laser Melting



**Department of Mining and Materials Engineering
McGill University, Montreal, Quebec**

Justin Mezzetta

August 2016

A thesis submitted to McGill University in partial fulfillment of the requirements needed to obtain a Master of Engineering from the Department of Mining and Materials Engineering

Abstract

The selective laser melting (SLM) of TiAl6V4 has become an increasingly popular manufacturing option in the biomedical and aerospace fields, mainly due to its ability to create complex, net-shape parts within a short amount of time. To eventually incorporate additive manufacturing techniques like SLM into common manufacturing practice, it is imperative to ensure that the mechanical behaviour and performance of selective laser melted TiAl6V4 parts has the consistency of wrought material, especially for safety critical applications. This work explored the optimization of SLM machine parameters, such as laser power and laser scan speed in order to achieve maximum density. With optimized parameters, densities exceeding 99.5% were obtained for SLM parts. Afterwards, a series of post-SLM heat treatments were applied to tensile test specimens, to observe their effects on microstructure and mechanical properties. Through hot-isostatic-pressing (HIP), SLM yield strength values exceeded the wrought reference of 880 MPa. HIPed tensile specimens also surpassed the wrought reference for final elongation (14%) in many samples. As anisotropy in mechanical properties of SLM parts have been reported in previous works, crystal orientation and its effect on mechanical properties is discussed.

Résumé

La fusion laser sélective (SLM) de TiAl6V4 est devenue une option de fabrication de plus en plus populaire dans les domaines biomédical et de l'aérospatiale, principalement en raison de sa capacité à créer, dans un court laps de temps, des pièces complexes en forme de filet. Afin d'incorporer éventuellement des techniques de fabrication d'additifs, tels que la SLM, dans la pratique de fabrication commune, il est impératif que le comportement mécanique ainsi que la performance des pièces TiAl6V4 aient une consistance qui correspond à celle du matériau forgé, en particulier pour les applications où la sécurité est cruciale. Ce travail a exploré l'optimisation des paramètres de la machine fusion laser, tels que la puissance du laser et la vitesse du balayage laser, afin d'obtenir une densité maximale. Avec des paramètres optimisés, une densité supérieure à 99,5% a été obtenue pour les pièces SLM. Par la suite, post-SLM, les spécimens ont été soumis à une série de traitements thermiques pour observer leurs effets sur la microstructure et les propriétés mécaniques. Grâce à la hot-isostatic-pressing (HIP), les valeurs de limite d'élasticité des spécimens SLM ont dépassé la référence forgé de 880 MPa. Les spécimens traités avec HIP ont également dépassé la référence forgé pour l'allongement final (14%) dans de nombreux échantillons. Comme anisotropie dans les propriétés mécaniques des pièces SLM ont été rapportés dans les travaux précédents, l'orientation cristalline et son effet sur les propriétés mécaniques ont également été discutés.

Acknowledgements

First and foremost, I would like to thank my supervisor, Professor Mathieu Brochu, for providing me with an exciting master's project and a great group of people to work alongside. Your helpfulness and continued guidance were essential to both my research and professional development as an engineer.

During my time in Professor Brochu's P²[AM]² research group, I have had the privilege of collaborating with many hard-working and talented individuals. I would like to extend special thanks to Jason Milligan, David Walker and Lucie Nguyen for helping me integrate when I first arrived at McGill and for transferring to me skills that would prove invaluable over the course of my master's research. Next, I'd like to thank Nejib Chekir and Jason Danovitch for contributing to my research with their expertise in welding and texture characterization. Additional thanks to Abhi Ghosh, Ryan Chou, Phil Hendrickx, Samantha Rudinsky, Andrew Walker, Bamidele Akinrinlola, Javier Arreguin, Jose Muñiz and Masum Tuncay, as well as the aforementioned, for making my experience at McGill a fun and memorable one! Also, thanks to Rodrigo Trespalacio, Shane Cavalluzzi and Dong-Geun Kim for keeping my soccer skills sharp for the day when I make the Montreal Impact.

Along with my research group, I owe a big thanks to Sergio and Igor Armano of Edmit Industries in Châteauguay. Your manufacturing expertise greatly facilitated the production of my thesis samples and it was great working with you. I'd also like to thank Andrea, Pavlo, Elmer, Michel, Marc-Michel, Johanne, Alex, and the whole staff at Edmit for making my time at Edmit a positive one!

In addition, thanks to everyone involved in the MANU 601 project for your helpful advice. Your collaboration with me on my research was greatly appreciated!

Finally, I would like to thank my family for all their support, encouragement and kindness throughout my life. I thank my father John Mezzetta and my mother Charlene Eldridge for their unwavering support, guidance and for the pride they take in my accomplishments. Special thanks to my brother Michael Mezzetta and my sister Kayla Mezzetta for all of the fun times

growing up and for being two of my closest friends. Great thanks to my grandparents Emilio and Angela Mezzetta and William and Callista Eldridge for their continuous love, kindness and interest in my life.

Table of Contents

Abstract	i
Acknowledgements	iii
Table of Contents	v
List of Figures	vii
List of Tables	ix

Chapter 1: Introduction

1.1 Additive Manufacturing	1
1.2 Selective Laser Melting	1
1.3 Ti6Al4V	3
1.4 Thesis Objective	3
1.5 Thesis Outline	3
1.6 References	4

Chapter 2: Literature Review

2.1 Additive Manufacturing Overview and General Process	5
2.2 Advantages of Additive Manufacturing	9
2.3 Drawbacks to Additive Manufacturing	10
2.4 Selective Laser Melting	11
2.5 SLM Machine Build Parameters	12
2.6 General Overview of Titanium	21
2.7 Crystal Structure of Titanium	23
2.8 Titanium Alloys	24
2.9 Ti6Al4V	26
2.10 Microstructure of Conventionally Processed Ti6Al4V	26
2.11 SLM Processed Ti6Al4V Microstructure	28
2.12 Defects in SLM of Ti6Al4V4	31
2.13 Heat Treatment of Ti6Al4V	31
2.14 Mechanical Properties of Selectively Laser Melted Ti6Al4V4	36
2.15 References	38

Chapter 3: Experimental Methods

3.1 Introduction	43
3.2 SLM Machine	43
3.3 Part Orientation	44
3.4 Post-Processing Treatments	45
3.5 Sample Fabrication and Post-Processing	45

3.6 Tensile Testing of Coupons	47
3.7 Porosity Measurement	48
3.8 Microstructural Analysis	48
Chapter 4: Structure and Property Relationships associated with Selective Laser Melting of Ti6Al4V	
4.1 Introduction	51
4.2 Experimental Methodology	53
4.3 Results and Discussion	55
4.3.1 Evaluation of Density	55
4.3.2 Microstructure	55
4.3.3 Mechanical Properties	61
4.3.4 Fracture Surfaces	65
4.4 Conclusions	67
4.5 References	68
Chapter 5: Summary	72

List of Figures

Figure 1.1: Examples of components fabricated through SLM, (a) a biomedical skull implant, (b) tool insert for auto part injection mould, (c) jet engine turbine blades	2
Figure 2.1: Schematic of Hull’s SLA apparatus specified in US patent 4.575.330	5
Figure 2.2: CAD model of a cup (a), and STL conversion of original CAD model (b)	7
Figure 2.3: SLM machine component layout	12
Figure 2.4: Density versus energy density curve for different stainless steels	14
Figure 2.5: Optical Absorption % (absorptivity) of selected metals vs. wavelength	15
Figure 2.6: (a) Porosity formed between scan vectors because of overly wide hatching distances [13] and (b) hatching distance influence on porosity	17
Figure 2.7: (a) Effect of scanning strategy on the relative density for Ti6Al4V Material and (b) schematic of applied scanning strategy	18
Figure 2.8: Island scan strategy employed on Concept Laser M2 SLM machine	19
Figure 2.9: Example of the effect of layer thickness on final build resolution	20
Figure 2.10: Schematic of staircase effect characteristic of SLM process	21
Figure 2.11: Schematic of Titanium Sponge Production from Rutile using Kroll’s Process	22
Figure 2.12: Appearance of atom structure for the alpha phase (a) and beta phase (b), with graph depicting transformation of phases for pure titanium (c)	24
Figure 2.13: Crystal lattice parameters for α phase (a) and β phase (b)	24
Figure 2.14: Phase diagrams for α stabilizing alloying elements (a), β stabilizing alloying elements (b,c) and neutral alloying elements (d)	25
Figure 2.15: Ti6Al4V Lamellar Microstructure	27
Figure 2.16: Development of Ti6Al4V Lamellar Microstructure	28
Figure 2.17: Columnar grains in SLM specimen	29
Figure 2.18: SEM image of α' martensite needles in as-built SLM condition	30
Figure 2.19: (a) and (b): Micrographs of SLM produced specimen, representing initial porosity	31
Figure 2.20: Relationship between time and amount of residual stress relief at various stress-relief anneal temperatures for Ti6Al4V alpha-beta alloy	33
Figure 3.1: M2 Cusing SLM machine by Concept Laser	43
Figure 3.2: Example of samples built in (a) Z, (b) X and (c) 45° orientations on build plate	44
Figure 3.3: ASTM E8M –04 dimensions used to fabricated tensile coupons	46
Figure 3.4: As-built tensile coupons built in the 45° (a), x (b) and z (c) orientations	47
Figure 3.5: Nabertherm argon furnace (a) and American Isostatic HIP furnace (b) used in post-processing of the as-built samples	48
Figure 4.1: SEM images of gas atomized Ti6Al4V powder particles	53
Figure 4.2: Optical micrograph depicting columnar grains in (a) X-built tensile samples, b) 45° built tensile samples and (c) Z-built tensile samples, with loading direction for tensile testing specified	57
Figure 4.3: Microstructures in the (a) stress relief, (b) mill anneal and (c) HIP conditions, respectively, with corresponding XRD spectra (d,e,f)	59

Figure 4.4: EBSD texture analysis conducted on the Ti- α phase of a side view of a tensile sample built in the z-direction, with the direction of pull oriented in the horizontal axis, showing (a) IPF map normal to plane, (b) pole figures for three main crystal orientations in the HCP system, and (c) corresponding IPFs	60
Figure 4.5: EBSD texture analysis conducted on the Ti- α phase of a top view of a tensile sample built in the x-direction, with the direction of pull oriented in the axis normal, showing (a) IPF map normal to plane, (b) pole figures for three main crystal orientations in the HCP system, and (c) corresponding IPFs	61
Figure 4.6: Ultimate Tensile Strength versus Yield Strength for Stress Relief, Mill Anneal and HIP conditions in X, 45° and Z build directions compared to existing values from literature	63
Figure 4.7: Ultimate Tensile Strength versus Final Elongation for Stress Relief, Mill Anneal and HIP conditions in X, 45° and Z build directions compared to existing values from literature	64
Figure 4.8: Fracture of HIPed X-oriented sample (a), versus HIPed Z-oriented sample (b)	66
Figure 4.9: SEM images for fracture surface of HIP X sample (a,c) and HIP Z sample (b,d)	66

List of Tables

Table 2.1: Additive manufacturing technologies	6
Table 2.2: Summary of annealing heat treatments for alpha-beta alloys, where T_{β} is the β -transus temperature of the particular alloy in question	34
Table 2.3: Effect of solution treating temperature on tensile properties of Ti6Al4V barstock	35
Table 2.4: As-built mechanical properties of SLM Ti6Al4V in literature	36
Table 3.1: List of technical data for M2 Cusing SLM machine	44
Table 3.2: Test Matrix of samples	46
Table 3.3: Grinding and polishing procedure for sample preparation	48
Table 4.1: Ti6Al4V Alloy Composition; data provided by the supplier	54
Table 4.2: SLM Part Porosity after Experimental Heat Treatments	55
Table 4.3: Vickers hardness for experimental samples	62

Chapter 1: Introduction

1.1 Additive Manufacturing

Additive manufacturing (AM) is a family of manufacturing processes that fabricate parts through the addition of material. AM machines use digital computer aided design (CAD) models, in conjunction with slicing algorithms, to form near net-shape parts. Each AM process has a unique method of forming parts; however the working principle remains the same: parts are formed through the layer-by-layer addition of material directly on an initial substrate. A wide variety of AM techniques are currently available, having the ability to process many different types of metals, ceramics and polymers. Through bonding of the layers, and having the ability to control the shape of finite layers, AM can produce consolidated working parts with relatively good accuracy. Because of the cross-sectional control of the building layers, a wide variety of geometries can be processed through AM. This gives engineers and designers an almost unlimited degree of freedom when designing components to be fabricated with AM.

The AM industry has seen steady economic growth in recent years, with reports estimating a market worth of 5.1 billion dollars in 2016 [1.1]. This is up from 3.1 billion dollars in 2014 [1.2]. Every year more companies are releasing industrial grade AM machines to the market, with the total number of AM machine manufacturers jumping to 62 in 2016 from 31 in 2011 [1.2]. The need for prototyping and innovative design in fields like aerospace and tooling have bolstered continued growth in AM, along with increased mainstream consumer interest in less-expensive desktop style AM machines for personal use.

1.2 Selective Laser Melting

Selective laser melting (SLM) is an AM process first developed in the mid 1990's. Physicists Dr. Matthias Fockele and Dr. Dieter Schwarze founded a German-based company F&S GmbH, which worked towards creating a process to form net-shape metallic parts using highly powered laser beams and fine metallic powders [1.3]. After years of development, F&S GmbH released the first commercially available SLM machine to the open market in 1999.

Since then, many different companies have begun to manufacture and distribute SLM systems that are capable of processing various types of metals. The main manufacturers of SLM machines today are: EOS, 3D Systems, Concept, Renishaw, SLM Solutions and Phenix [1.4]. Common metals processed on these machines include titanium, aluminum, various grades of steel, cobalt-chrome and nickel alloys [1.5]. Initially used for rapid prototyping (RP), modern SLM machines are now being used to create functional, end-use parts due to the process' ability to achieve near full density [1.6]. The SLM of metals has sparked particular interest in the biomedical, tooling and aerospace fields, where customizability and weight savings are of utmost importance. Figure 1 displays several examples of modern products fabricated through SLM. Figure 1.1 (a) shows a custom skull implant fabricated from a scanned CAD model of a fractured skull. Implants are often specific to the individual, making the SLM process a useful tool in the biomedical field. In Figure 1.1 (b), a tooling insert for an auto part injection mould is shown. The more efficient helical internal cooling channels would be extremely difficult to fabricate through traditional modes of manufacturing. Figure 1.1 (c) shows a jet engine turbine made from Ti6Al4V. The turbine was built in a single net-shape build through SLM, eliminating the need for moulding and multiple-stage machining.

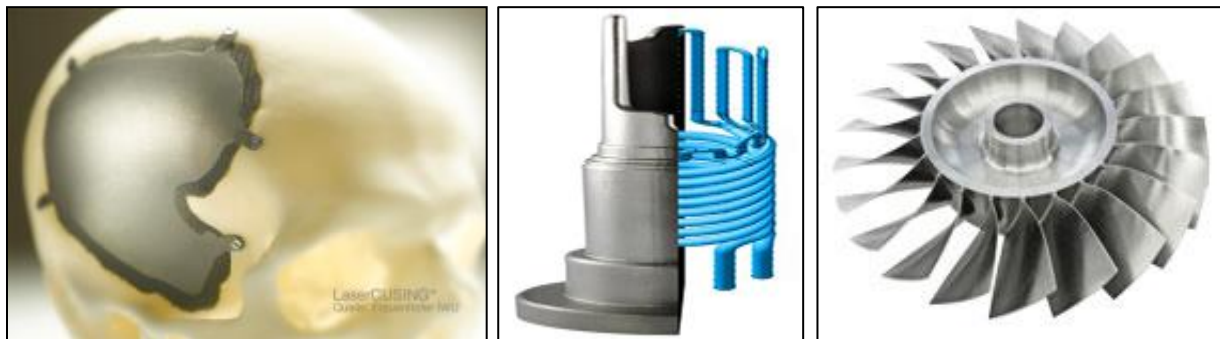


Figure 1.1: Examples of components fabricated through SLM, (a) a biomedical skull implant, (b) tool insert for auto part injection mould, (c) jet engine turbine blades [1.7]

1.3 Ti6Al4V

Ti6Al4V is the workhorse for the titanium industry and accounts for over 50% of all titanium production. It is a popular choice in many applications due to its excellent combination of strength, toughness and corrosion resistance [1.8]. Typical uses include aerospace applications like pressure vessels, gas turbine disks, cases and compressor blades [1.8]. Ti6Al4V has also seen application for surgical implants in the biomedical field, due to its high strength/weight ratio and biocompatibility with the human body. In this context, the AM of Ti6Al4V is of particular interest for the many potential applications that require complex geometry, good strength and light service weight.

1.4 Thesis Objective

This thesis project aims to provide insight on process-property relationships seen for the SLM of Ti6Al4V alloy. Previous works have shown that as-built SLM specimens of this alloy have high strength but low ductility when compared to wrought Ti6Al4V. Given that SLM parts have properties different from those of traditionally cast and wrought materials, it is important to test and document SLM properties so that they may be better understood for future applications

Since the as-built mechanical properties of SLMed Ti6Al4V are quite well documented in existing literature, this study will primarily focus on the refinement of as-built part properties through post-processing. Resulting mechanical properties from post-process treatments will be benchmarked against current ASTM standards for powder bed fusion of Ti6Al4V (ASTM F2924) [1.9], as well as with AMS standard wrought material values (AMS 4911) [1.10]. This study will also heavily focus on the microstructures of different post-process heat treatments to better understand the relationships dictating the mechanical behaviour.

1.5 Thesis Outline

The works in this thesis will be presented in 4 chapters including

- Literature review, the literature review will give an overview of the SLM process, the metallurgy of Ti-6Al-V4 and results obtained in other SLM studies of this alloy.

- Experimental methods, where the experimental strategy, along with the methods and equipment used to examine material and mechanical properties will be described in detail.
- Results and discussion, packaged under a proposed scientific paper entitled “Structure and Property Relationships associated with Selective Laser Melting of Ti6Al4V”. The scientific paper will compare mechanical and material properties obtained from the study and discuss the effect had on the SLM parts from post-processing and build orientation.
- Summary, where the findings from this body of work will be discussed in the final chapter.

1.6 References

- [1.3] Wohlers, Terry. *Past, Present and Future Of Rapid Prototyping*. IJPD 1.2 (2004): p. 147.
- [1.4] Kumar, Sanjay, and Sisa Pityana. *Laser-Based Additive Manufacturing Of Metals*. AMR 227 (2011): p 92-95.
- [1.5] Aziz, I. *Microstructure and mechanical properties of Ti6Al4V produced by selective laser sintering of prealloyed powders*. M. Eng. University of Wikato, 2010: p. 8
- [1.6] Vandenbroucke, B. and J.P. Kruth. *Selective Laser Melting Of Biocompatible Metals For Rapid Manufacturing Of Medical Parts*. Rapid Prototyping Journal 13.4 (2007): p. 196-203.
- [1.7] Concept-laser.de, *Laser Melting Metal, Additive Manufacturing - Aerospace Industry - Concept Laser*. N.p., 2015. Web. 20 Apr. 2015.
- [1.8] Donachie, M. *Titanium: A Technical Guide*. Materials Park, Ohio: ASM International, 2010. p. 2.
- [1.9] ASTM F2924-14, *Standard Specification for Additive Manufacturing Titanium-6 Aluminum-4 Vanadium with Powder Bed Fusion*, ASTM International, West Conshohocken, PA, 2014, www.astm.org
- [1.10] SAE AMS 4911, *Titanium Alloy, Sheet, Strip, and Plate, 6Al - 4V, Annealed*, SAE Aerospace.
- [1.11] Wohlers, T. *Wohlers Report 2016*, Wohlers Associates, 2016.
- [1.12] Wohlers, T. *Wohlers Report 2014*, Wohlers Associates, 2014.

Chapter 2: Literature Review

2.1 Additive Manufacturing Overview and General Process

The origin of modern commercial AM machines is commonly credited to Chuck Hull's US patent (4.575.330) for Stereolithography (SLA) in the mid 80's [2.1]. Hull's patent for the SLA machine specified a method for creating parts where ultraviolet (UV) light is used to cure liquid polymers in a layer-by-layer sequence until final parts are formed. To fabricate these parts, the SLA machine in the patent was shown to move a UV source so that it would trace and solidify a thin layer of liquid polymer in the shape of a desired 2-D cross section. The SLA machine then used an elevator to drop down the solidified layer and submerge it a vat of liquid polymer. The process would then iterate itself by curing another 2-D cross section, joining the top layer with the already solidified layer beneath. Hull stated that through many repetitions of these steps, final consolidated parts could be formed. A schematic of his patent is shown in Figure 2.1.

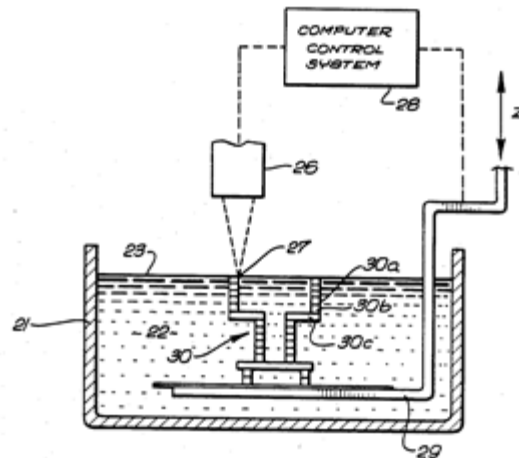


Figure 2.1: Schematic of Hull's SLA apparatus specified in US patent 4.575.330 [2.1].

After Hull created his first patent, many different AM technologies have since been patented and commercialized. These technologies have the capability to fabricate parts of many different materials, ranging from polymeric materials and waxes to composite materials, ceramics and metals. Although the technologies make use of different energy sources and means of depositing material, the main principal of combining thin layers of material together to create final shapes is consistent across all platforms. A list of modern day AM technologies used to

create metal and plastic parts is displayed in Table 2.1. Of these, Selective Laser Melting (SLM) will be described in depth later on, as it is the main focus of this study.

Table 2.1: Additive manufacturing technologies [2.1].

Technology	Acronym	Energy	Geometry	Plastic	Metal
Stereolithography	SLA	Laser	Scan	X	
Fused Deposition Modeling	FDM	Heat Extrusion	XYZ Kinetic	X	
3D Printing Drop on Bed	3DP	Binder	XYZ Kinetic	X	x
Selective Laser Sintering	SLS	Laser	Scan	X	x
Selective Laser Melting	SLM	Laser	Scan		x
Electron Beam Melting	EBM	Electron Beam	Scan		x

According to Gibson [2.2], manufacturing technologies under the AM classification share seven common steps:

1. Computer Aided Design (CAD)

All AM systems begin with the design of a solid 3D model using software capable of fully describing the external surfaces of the part to be made. Some popular modern 3D CAD software used in industry includes AutoCAD, Catia, Solidworks and Pro/ENGINEER. Reverse engineering scanning systems (i.e. laser scanning) can also be used to create digital 3D models from existing objects.

2. Conversion to STereoLithography (STL) File

Most all AM machine require input of a STereoLithography (STL) file. STL files are derivatives of CAD files, where 3D CAD models are translated into triangulated versions of the original.

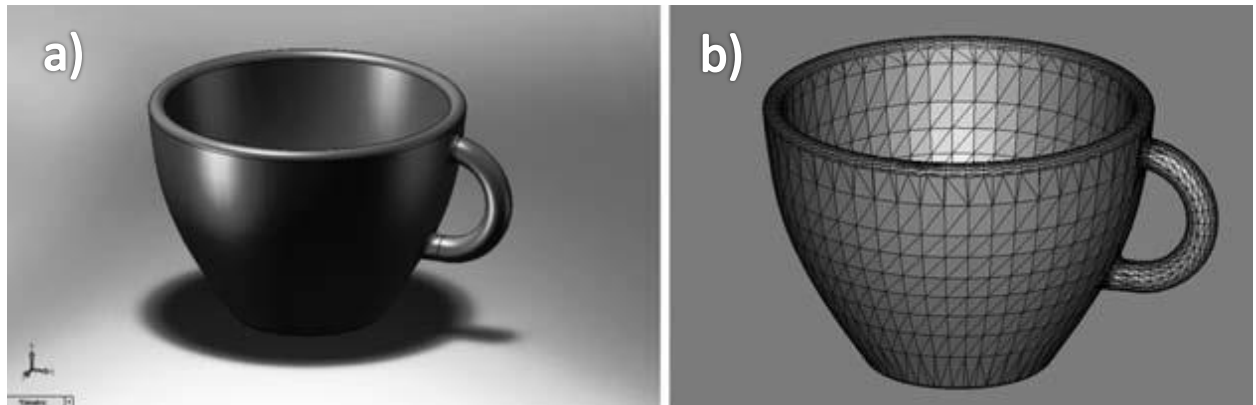


Figure 2.2: (a) CAD model of a cup, and (b) STL conversion of original CAD model [2.3].

Using triangulated geometry of the model's surface, mathematical slicing algorithms are able to calculate coordinates of 2D planes (or layers) within the 3D model. These coordinates are relayed to the motor control system of the AM machine and give directions on how to move in order to fabricate each layer. An example of an STL conversion can be seen in Figure 2.2.

3. Transfer to Additive Manufacturing Machine and STL File Manipulation

After conversion from CAD to STL file format, STL files are loaded on to the additive manufacturing machine. An interface on the machine allows user input, to decide where the STL model is placed on the build platform and how it is oriented. Depending on the machine, multiple STL models can be fabricated in the same build plate, providing that there is no cross-sectional overlap between any of the parts to be built.

4. Machine Setup

Before the AM machine begins to replicate the STL model, the machine must first be given instructions on how to build the part. Common user input parameters include power of the energy source, speed of build and individual thickness of each layer. Parameter selection is a key component to the AM process because machine parameters influence the build time and final quality of the part (dimensional accuracy, density, surface roughness etc.) [2.4,2.5,2.6].

5. Build

Once the build process has started, AM machines are fairly autonomous where parts are built with minimal supervision from start to finish. Machines are checked occasionally to verify that power outages, material deficits or software glitches have not interrupted the build.

6. Removal

After completion of the build, parts must be removed from the substrate on which they were built. Plastic parts built with photopolymer or extrusion AM machines can usually be removed by hand manually, however most parts made of metal must be removed through sawing or electro discharge machining. An exception to this would be when metal parts are built upon many thin, metal supporting rods, which are usually a fraction of a millimeter in diameter. These supports can be removed by hand with a hammer and metal wedge tool.

7. Post-Processing

Post-processing may be optional or required, depending on application requirements. For example, additive manufactured metal parts requiring high fatigue life may be surface machined or sanded down to reduce the likelihood of cracks initiating at rough surfaces created through AM processing. Machining is particularly important on surfaces that have been removed from supports, as these surfaces tend to have microvoids resulting from the support stilts. Machining is also required if the AM part requires any threads or a tighter tolerance than the AM process can provide for.

Along with surface finishing, additive manufactured parts are sometimes heat treated after fabrication. Heat treatments can serve to remove residual internal stresses from the AM process, or to optimize mechanical properties like strength and ductility.

8. Application

After post-processing, the additive manufactured part is ready for service. With increasing investment in to the research and development of AM, parts built through this process are continuously improving in terms of strength and overall mechanical properties. Because of design flexibility to build custom parts, AM is an increasingly popular option in today's manufacturing landscape.

2.2 Advantages of Additive Manufacturing

In recent years, AM has seen considerable growth in industries requiring complex parts, on a low volume production scale. Companies in the aerospace and biomedical industries have been prime users of AM technology, making use of AM's ability to fabricate complex near net-shape parts with little lead time compared to conventional means of manufacturing [2.8,2.9]. The following features make AM an attractive candidate for part fabrication:

- i) **Near Net-Shape Parts:** AM has the capability of producing near net-shape parts in its initial build. Traditional subtractive manufacturing requires multiple machining procedures to produce a final end-use part, whereas AM can fabricate the same part in fewer steps.
- ii) **Extremely Complex Parts:** Because of AM's layer by layer deposition sequence, virtually any shape part can be fabricated using AM. Intricate external and internal features can be made with AM that traditional machining cannot replicate due to inaccessibility of the cutting tool to access the region of the feature. AM also has the potential to replicate parts that were previously only capable of being manufactured by investment casting. An example of such a part would be turbine blades [2.9].
- iii) **Shorter Lead Times:** Lead times of AM are short compared to conventional manufacturing. AM machines are capable of commencing construction of parts immediately after the CAD design is complete. AM machines do not require the fabrication of die moulds as with injection moulding, or multiple steps in machining as with CNC machining. Once a product is conceptualized, AM machines have an

- extremely fast turnaround between visualization of the concept and a functioning prototype.
- iv) **Cost Effectiveness for Low Volume Parts:** For complex custom parts built in low quantities, the cost of producing individual parts with AM could be lower than with conventional die casting or CNC machining. Die casting requires manufacturing of the part die, while CNC machining scraps high amounts of metal before the final part is formed. Both of these conventional means of manufacturing are costly if parts are not made in mass production.
 - v) **Reduction of Material Waste:** To fabricate certain aerospace components, it has been reported that 90% of material is scrapped before the final part is formed [2.10]. With AM, almost all of the material can be recycled for subsequent builds and minimal material is lost during the AM lifecycle.

2.3 Drawbacks to Additive Manufacturing

While there are many benefits to using AM, a few drawbacks do exist. One of the issues for metal parts built through AM is that mechanical properties show a degree of anisotropy due to columnar grains and heavy texture, as well as weakness in bonding between layers [2.4, 2.11, 2.12]. This may lead to a variance in mechanical performance with loading direction, and suboptimal properties in cases where full bonding is not achieved. In the same vein, mechanical properties of AM produced samples are not standardized as extensively or consistently as cast or wrought materials, as the surface finish for testing often varies. This makes it difficult when designing parts to adequately account for loading and fatigue life conditions.

In terms of cost effectiveness, AM technologies are limited in the volume of parts they can produce in a given time. Because of low deposition rates and limited area available for parts on the build platform, many parts cannot be produced as fast with AM when compared to other manufacturing processes. For powder based AM processes, metals in powdered form are more expensive per unit mass than their bar stock equivalent. This is due to the additional processing required to convert base metal into a powdered form (usually through gas or water atomization). The higher material costs of powder based AM technologies makes it difficult to

compete with traditional casting and forging methods, when producing parts in high volumes [2.13]. An example of this would be titanium, where bar stock ranges from \$15-30/lb, while titanium powder costs anywhere from \$100-350/lb. AM in its current state is best suited for complex, customizable parts manufactured in low quantities.

2.4 Selective Laser Melting

The main focal point of this research is centered on Selective Laser Melting (SLM). SLM is an AM technique which uses a highly powered CO₂ or Nd:YAG laser beam to fully melt and fuse together thin layers of fine metallic or ceramic powder (usually ranging from 30-200 μm in particle size). SLM can process a variety of metals, including titanium, stainless steel, aluminum, nickel-based alloys and chromium cobalt. Unlike with solid state sintering, where densification occurs slowly from solid diffusion between powder particles, the laser energy in SLM fully melts solid powder to liquid, after which the molten metal pool quickly re-solidifies. This leads to complete joining between powder particles and nearly fully dense materials (99.5%+ density with Nd:YAG lasers) [2.14]. As with welding, one effect of the rapid melting-cooling cycle is a build-up of internal residual stresses in parts [2.12,2.15]. For this reason, post process heat treatments are required to relieve these stresses.

A schematic of the typical SLM process is shown in Figure 2.3. The process initiates when a coater blade spreads a thin layer of powder (typically 30-100 microns in thickness) over a metal plate resting atop a motor controlled piston. This plate commonly referred to as the build plate. The build plate is made of the same material as the powder, so that the printed part can properly bond to the plate and remain firmly fixed for the build duration. After the build plate is covered with a thin layer of powder, a laser is activated and an overhead scan box directs the laser on where to melt the powder bed using a series of mirrors. The laser path determines the shape of the thin cross-section, by fully melting and shortly thereafter re-solidifying the powder. After melting is complete, the laser is shut off and the build plate is dropped down by a fractional distance. The coater blade once again sweeps across the build platform and deposits a thin layer of powder onto the previously solidified cross-section or layer. Through many iterations of these steps, consolidated 3D objects are capable of being formed. In modern SLM,

build rates can range from 5-60 cm³ per hour, depending on the material being processed and the SLM machine [2.16, 2.17].

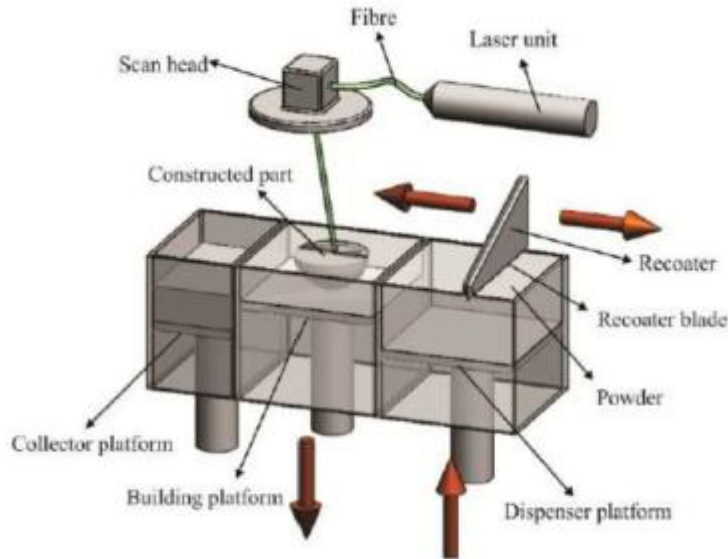


Figure 2.3: SLM machine component layout [2.18].

2.5 SLM Machine Build Parameters

Mechanical properties of SLM built parts are strongly influenced by the SLM machine parameters selected for building. In cases where machine parameters do not provide optimal energy to the powder bed, problems such as incomplete melting or unstable melt pools may arise. Micro-voids and increased porosity are typical in these conditions and often lead to mechanical deficiencies including reduced fatigue strength and poor ductility in parts. For this reason, industry leaders in SLM machinery invest heavily into research and development, so that their machine parameters are optimized to specific types of materials which give them the capability of producing fully dense parts.

The main parameters to consider on modern SLM machines for optimal melting and density include:

Chapter 2

- i) Laser Power
- ii) Laser Scan Speed
- iii) Hatching Distance
- iv) Layer Thickness

These parameters can be related to one another with a factor called Energy Density. The volume based Energy Density factor (J/mm^3) has a strong correlation to the final density of as-built SLM parts [2.19]. Energy Density is calculated as seen in Equation (2.1), where P is the laser power in Watts, v is the laser scanning speed in mm/s, h is the hatching distance between two adjacent scan vectors in mm, and t is the layer thickness, also measured in mm.

$$E = \frac{P}{v * h * t} \quad (2.1)$$

Figure 2.4 shows a relation between Energy Density and sample density through SLM of stainless steel powder [2.20]. It can be seen that part density steadily increases with Energy Density, until it levels off a point after 99%. Further increasing of Energy Density from that point on has little effect on density. This suggests that an optimal Energy Density can be obtained, so that excessive power or slower than needed scan speeds are avoided.

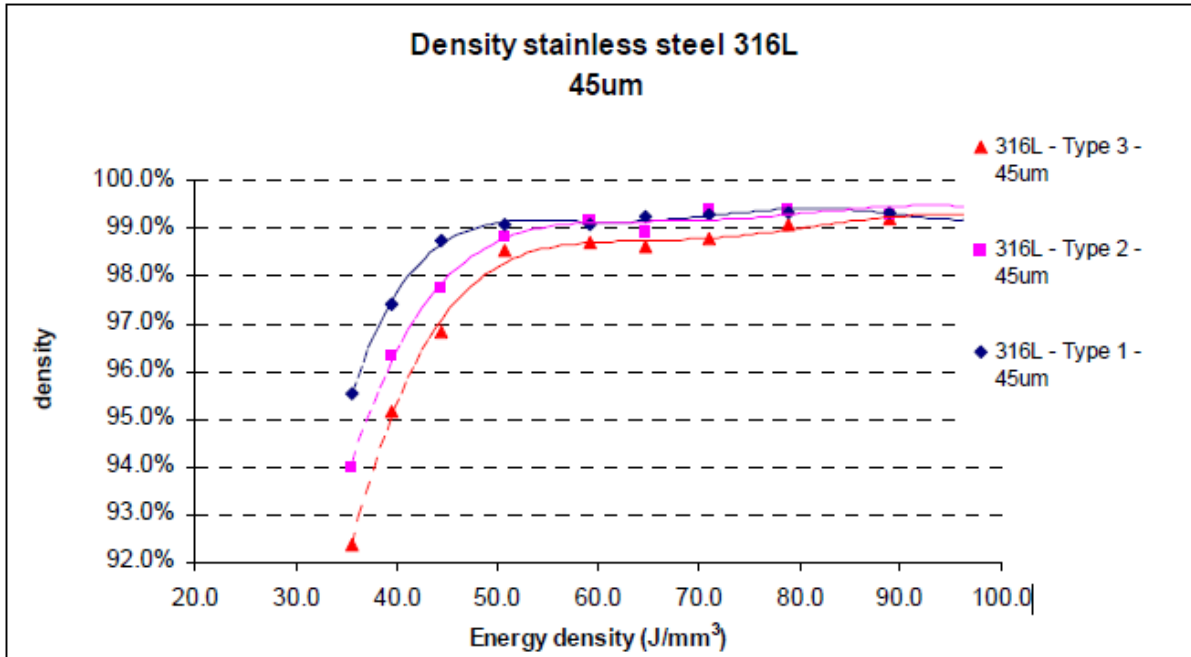


Figure 2.4: Density versus energy density curve for different stainless steels [2.20].

The effects of machine parameters shown in Equation (1) on SLM parts will be further discussed in the proceeding section.

Laser Power

Laser power is a term used to describe the rate of light energy delivered to the powder bed, measured in Watts, or Joules per second. Laser power is a critical SLM machine parameter because it is highly influential on an SLM part's quality. Lower powers have to be compensated for with slower scanning speeds, which effectively lowers the build rate of the part. If laser power is too low, and scanning speeds are too high to compensate, insufficient energy will be delivered to the powder bed. This will result in highly porous parts due to incomplete melting and bonding of powder particles.

The first type of lasers integrated into initial SLM machines were CO₂ lasers, however they had limited success in achieving high density. As a result, more recent SLM machines have incorporated Nd:YAG lasers into their systems. The transition to using Nd:YAG lasers was driven by the fact that metals absorb energy more readily when interacted with laser energy of

smaller wavelengths [2.21]. This relationship is shown for various different metals in Figure 2.5. Higher absorption of the energy into the metal allows powder particles to reach their melting temperatures more rapidly and create a fully melted, continuous weld pool as the laser traverses the powder bed.

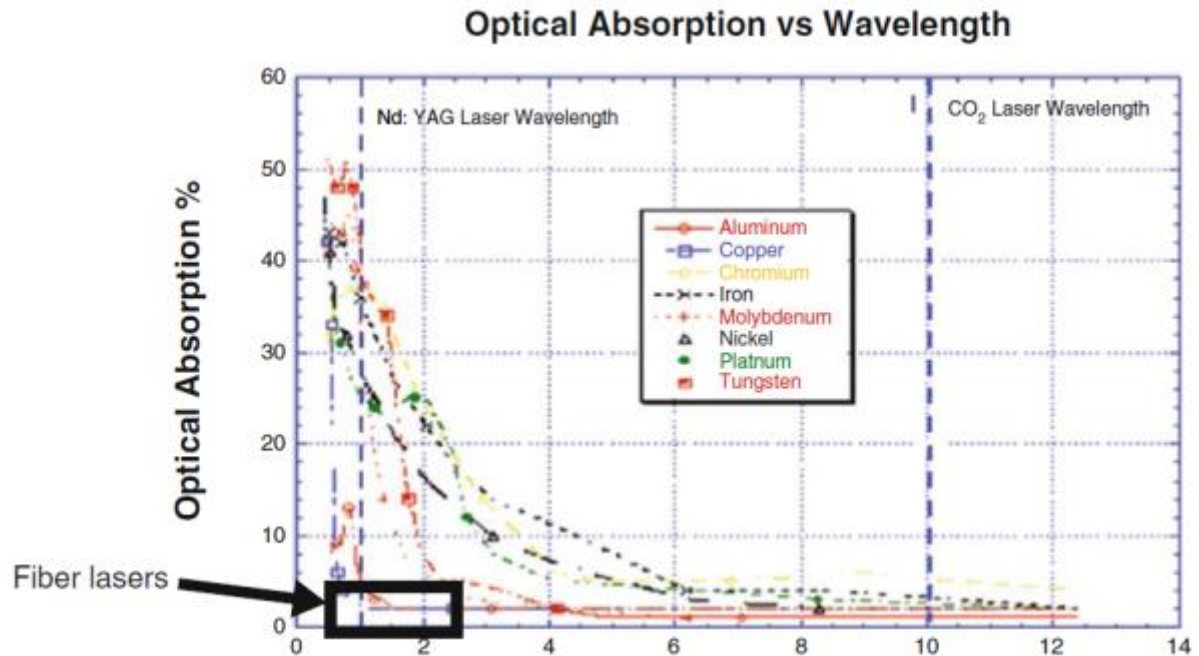


Figure 2.5: Optical Absorption % (absorptivity) of selected metals vs. wavelength [2.22].

The power level for SLM fabricated metal parts usually falls within the 50-400 Watt range for continuous wave Nd:YAG lasers [2.23]. Selection of power level depends on many different factors, including: the thermal conductivity of the material, the stability of the melt pool, the processing time a manufacturer is willing to commit to a part, as well as the acceptable density of final parts.

Laser Scan Speed

In SLM, a laser scan speed is defined as the rate at which a laser travels across a powder bed. By using motor-controlled mirrors, lasers beams are capable of being deflected to achieve high scanning speeds. Modern SLM machines offer laser scan speeds ranging from 0.1-10 m/s [2.16, 2.17]. Most SLM studies to date have used 0.1-1.5 m/s [2.23].

High scan speeds promote faster build rates and better productivity, however there are certain drawbacks. One is that high scan speeds can create melt pool instabilities [2.19]. Due to shear forces present at high scan speeds, there may be high surface tensions across the melt pool. Molten surfaces have an affinity to “ball up” in order to reduce surface tension. Under rapid solidification, these balls solidify in spherical form and protrude from the SLM part surface. These balls may increase the surface roughness of SLM samples [2.24, 2.25, 2.26]. Another issue with high scan speeds is that high shear forces may eject bits of molten metal from the melt pool [2.19]. Missing material from the melt pools has been said to form internal pores and effectively reduces the final density.

Hatching Distance and Scanning Strategy

Laser beams on SLM machines work to melt and re-solidify layers of powder, fusing powder particles together and creating solid slices. Although the laser can be deflected in many different ways to form these solid slices, the manner in which the laser beam traverses the powder bed has a large effect on material properties.

The main two factors to consider on a laser’s path across a powder bed are:

- i) Hatching Distance
- ii) Laser Scanning Strategy

Hatching distance is defined as the spacing between the centers of two adjacent laser scan vectors [2.27]. Along with being tied to the overall energy input [2.19], hatching distance plays a key role in achieving full melting of powder particles. Having a full, continuous melt is imperative to creating high density parts through SLM [2.28]. It has been seen in literature that having too large a hatching distance relative to the laser spot size will result in unmelted powder particles existing between laser scan vectors [2.24, 2.25]. Unmelted powder due to overly wide hatching distances often results in porosity between adjacent scanning vectors. This porosity between laser tracks can be seen in Figure 2.6 (a).

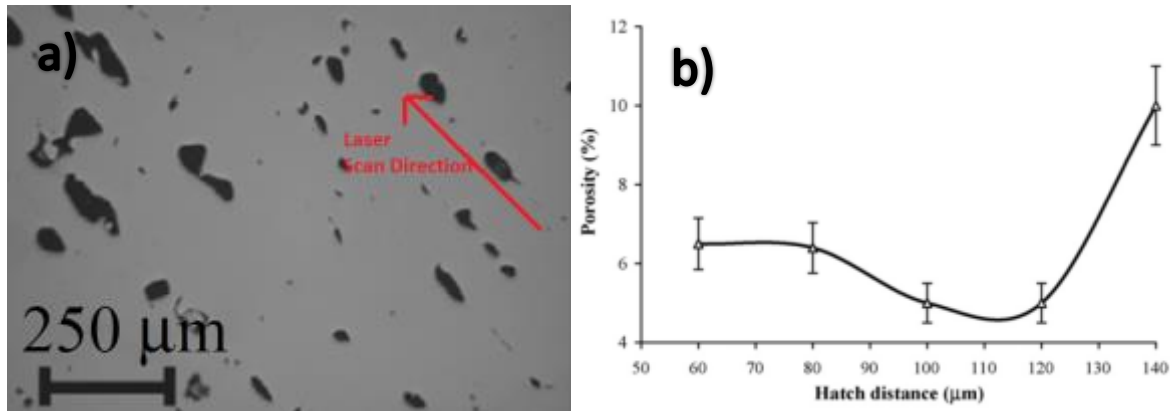


Figure 2.6: (a) Porosity formed between scan vectors because of overly wide hatching distances [13] and (b) hatching distance influence on porosity [2.24].

On the other end of the spectrum, minimizing hatching distance to under a certain point will have a similar effect in increasing porosity [2.25, 2.28]. By having smaller hatching distances, more of the laser's focal point interacts with previously solidified scan vectors, because of overlap between the vectors. Already solidified laser vectors have a tendency to be heat sinks. Hence with smaller hatching distances and higher overlapping, more of the laser energy will get conducted away into the metal, which results in less energy available to the melt the powder adjacent to the already solidified metal. A plot showing a relationship between porosity and hatching distance for the SLM of nickel powder is shown in Figure 2.6 (b). This work [2.24] suggests an optimal hatching distance must be selected to achieve the highest possible density.

Along with porosity, another issue in SLM is the high amount of internal residual stress induced into parts during processing. Residual stresses are detrimental to SLM builds because they may cause parts to fail during building. They can also negatively affect mechanical properties like fatigue strength and life [2.15]. To counteract build-up of residual stresses, SLM machines commonly employ strategic laser scanning paths which aim to limit heat build-up and thermal expansion/contraction. An example of a laser scanning strategy is seen in Figure 2.7. This particular laser strategy scans parts in a series of randomized islands. By building in a sequence where no two touching islands are built consecutively, heat build-up is controlled and stresses are minimized [2.4]. Some other types of scanning strategies investigated in literature include uni-directional, zig-zag and alternating zig-zag [2.64]. Depending on the type of scanning strategy employed, variations in density are noted. Figure 2.8 shows different scanning

strategies and their respective densities. Alternating zig-zag patterns have high densities which can be attributed to the strategy being more unlikely to have unmelted powder between scan tracks when compared to other strategies [2.64].

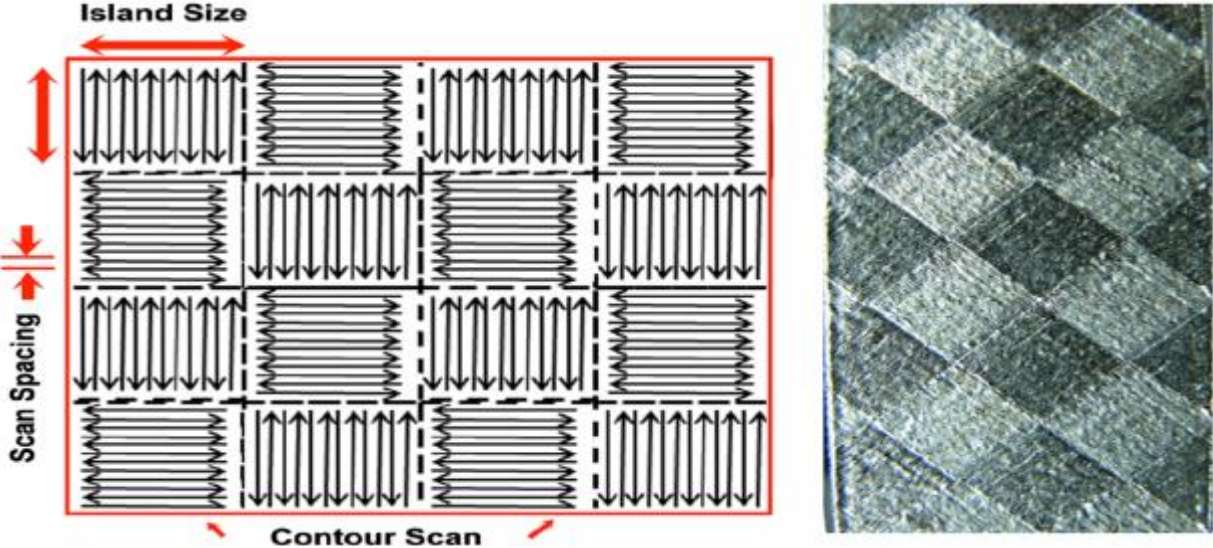


Figure 2.7: Island scan strategy employed on Concept Laser M2 SLM machine [2.4].

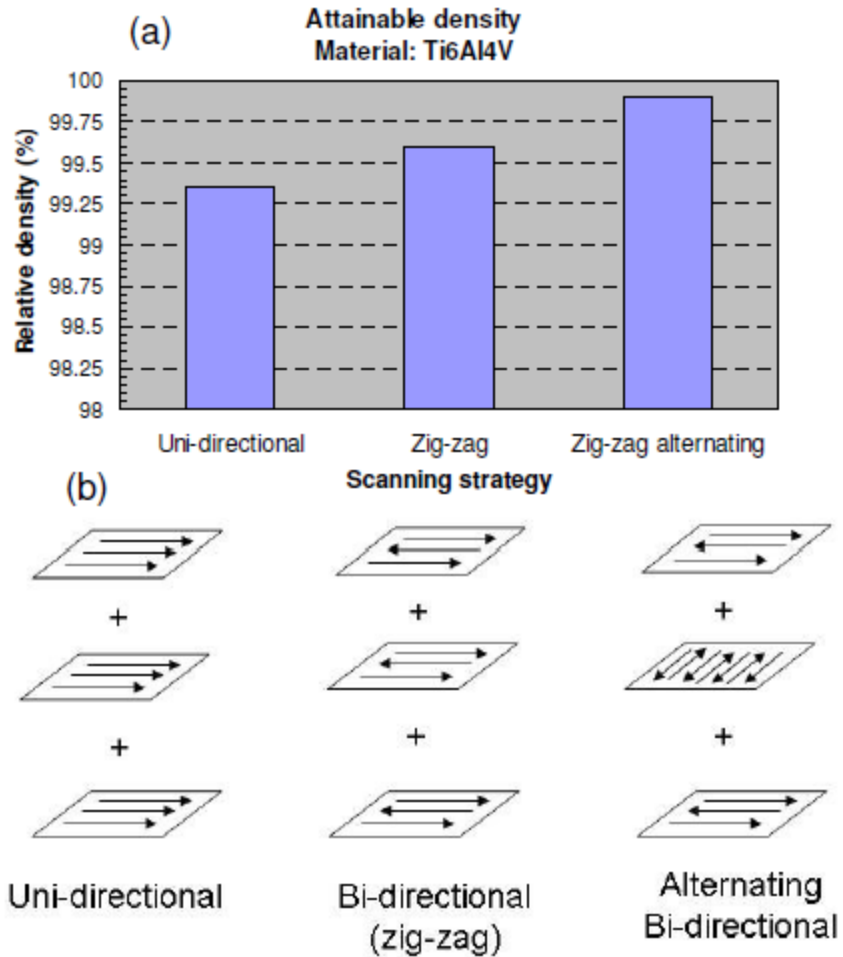


Figure 2.8: (a) Effect of scanning strategy on the relative density for Ti6Al4V Material and (b) schematic of applied scanning strategy [2.64]

Layer Thickness

Layer thickness is defined as the thickness of each deposited layer of powder, and is an important process parameter to consider when building parts through SLM. Due to the layer-by-layer nature of the SLM process, layer thickness has an influence on many properties of final parts, including accuracy, resolution and surface roughness [2.26. 2.29]. It also has an influence on the processing time of built parts, as SLM parts can be built faster when increasing layer thickness (i.e. fewer layers needed to fabricate final part).

As stated, accuracy and resolution of an SLM built part with respect to an original CAD model is highly dependent on layer thickness. An example of the relationship between accuracy and layer thickness can be seen in Figure 2.9, where a cup is built using different layer thicknesses

[2.30]. From the picture, it is seen that the cup produced using thicker layers has a much lower accuracy when compared to the one built with thinner layers. The difference in accuracy is attributed to the “stair-case” effect [2.26].



Figure 2.9: Example of the effect of layer thickness on final build resolution [2.30].

The stair-case effect is prominent in SLM because curves in the process are formed by slight overlapping differences between layers. The larger each layer, the larger the “step” and hence, the rougher a curved surface will be. A schematic of the staircase effect and surface roughness for a curved SLM surface is shown in Figure 2.10.

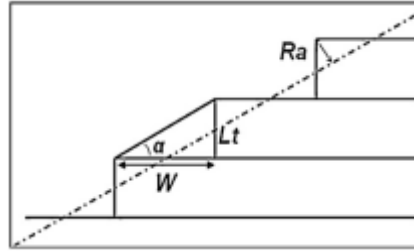


Figure 2.10: Schematic of staircase effect characteristic of SLM process [2.26].

2.6 General Overview of Titanium

In 1791, the element that later became known as titanium was first observed by the amateur mineralogist William Gregor. In his studying of iron-sand (FeTiO_3), he noted the presence of an unidentified element embedded in the mineral. Several years later, in 1795, German chemist Martin Klaproth took note of the same unknown element while examining rutile minerals (TiO_2). It was Klaproth who characterized the element and eventually denoted it as Titanium.

In terms of quantity, Titanium is the 9th most abundant element found in Earth's crust. Compared to structural metals, it is the 4th most abundant following iron, aluminum and magnesium. Within Earth's crust, titanium is found in many different, naturally occurring minerals. The most economically feasible ores used in titanium production today are ilmenite (FeTiO_3) and rutile (TiO_2).

Although titanium has been known to be present in these ores for quite some time, commercialization of the metal didn't occur until the advent of Kroll's process at the mid-point of the 20th century. William Kroll, inventor of Kroll's process, designed a system in which pure, ductile titanium could be extracted from ore in the following steps:

- 1 - The ore is first chlorinated to form a product of TiCl_4 .
- 2 - TiCl_4 is distilled to high purity.
- 3 – Purified TiCl_4 is reduced with magnesium within an inert gas chamber at high temperatures.

By reducing TiCl_4 with Mg in an inert environment at highly elevated temperatures (800-1000°C), a highly pure titanium metal in a “sponge-like” form can be produced. A schematic of

the Kroll's based process that produces sponge titanium from rutile ore can be seen in Figure 2.11. From the sponge, titanium and titanium alloy ingots are formed through arc-melting of the sponge in an inert environment. Ingots are further worked to obtain optimal mechanical properties for application.

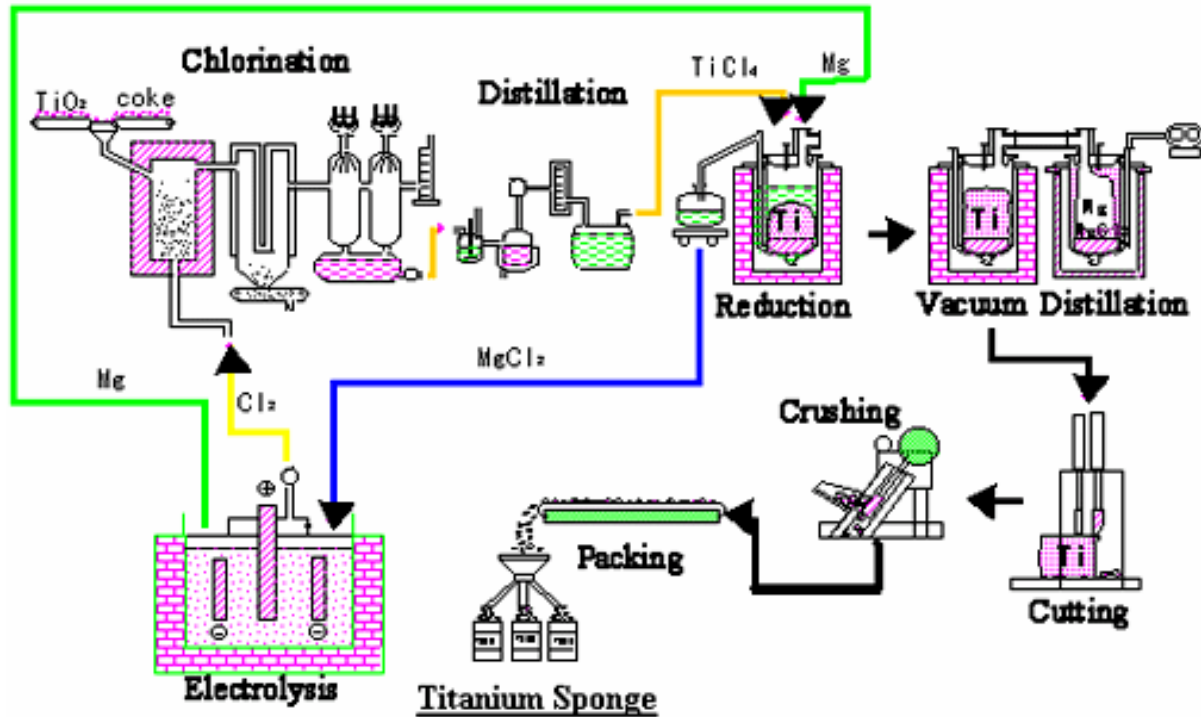


Figure 2.11: Schematic of Titanium Sponge Production from Rutile using Kroll's Process [2.31].

In today's industrial landscape, although expensive to produce, titanium has found a niche in many industries owing to its unique density, high temperature performance, excellent corrosion resistance and high specific strength when compared to competing structural metals like steel, aluminum and the superalloys [2.34]. The aerospace industry was the first to utilize titanium in large quantities and continues to be the largest consumer of titanium today. Titanium turbine blades are commonly found in jet engines on airplanes due to the material's high strength to weight ratio. Recently, titanium has seen increasing usage over other materials in heavily loaded aircraft components like fasteners and landing gears. Supersonic military jets

have made use of titanium skins to insulate aluminum airframes from high temperatures generated by supersonic flight.

Along with aerospace, the biomedical industry is a big user of titanium in their production of implants. Titanium is well suited for biocompatible implants because of its excellent corrosion resistance, non-magnetic properties and extreme light weight when compared to other metals used in implant products (stainless steel, chromium cobalt alloys). In recent years, titanium alloys have seen use in the fabrication of cardiovascular, orthopaedic and dental implants [2.32].

2.7 Crystal Structure of Titanium

Titanium is an allotropic element that can exist in two different crystallographic arrangements. Depending on the temperature, titanium atoms will arrange themselves in one of two crystal forms. From room temperature until 882.5 °C, titanium has a hexagonal close packed (hcp) crystal structure. This hcp arrangement in titanium is commonly referred to as the alpha (α) phase. When titanium is heated and exceeds a temperature of 882.5 °C, the alpha phase transforms into a body centered cubic (bcc) crystal structure, which is referred to as the beta (β) phase [2.33]. This transformation temperature of 882.5 °C is known as the β transus temperature.

The unit cells of both α and β phases are shown in Figure 2.13. In the α phase unit cell, the most densely packed lattice planes are the basal (0001), prismatic {1010} and pyramidal {1011} planes [2.33]. For the β phase unit cell, the most densely packed planes are the six planes found in the {110} family of equivalent symmetrical planes. Atomic spacing lattice parameters are $a=0.295$ nm, $c=0.468$ nm for the α unit cell and $a=0.332$ nm for the β unit cell [2.33].

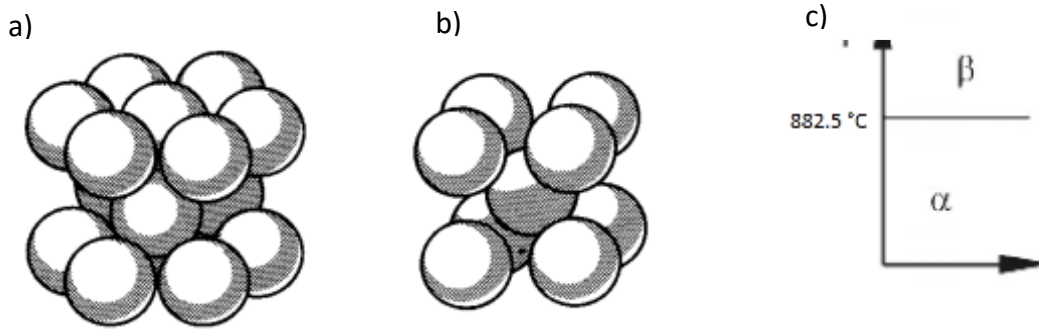


Figure 2.12: Appearance of atom structure for (a) the alpha phase and (b) beta phase (b), with (c) graph depicting transformation of phases for pure titanium [2.34].

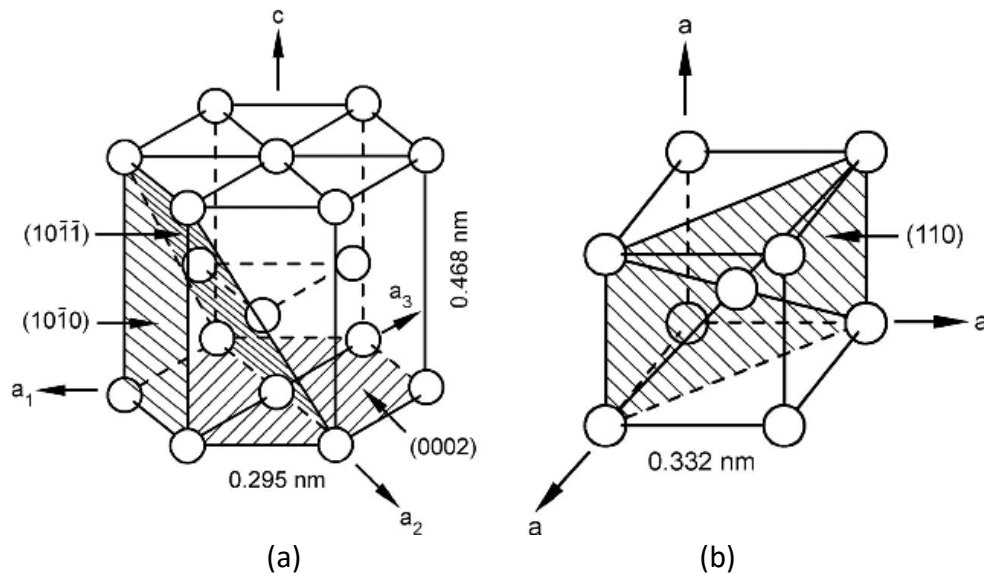


Figure 2.13: Crystal lattice parameters for α phase (a) and β phase (b) [2.33].

2.8 Titanium Alloys

Commercially pure (CP) titanium at room temperature has a final microstructure consisting entirely of α phase. This can be seen in Figure 2.12 (c), where titanium below the β transus temperature of 882.5 °C will revert back to the α phase after cooling [2.34]. In terms of properties, CP titanium has good ductility (20-25%), yet only possesses a moderate ultimate tensile strength (200-600 MPa) [2.61] when comparing to steels and super alloys. To obtain a

good mixture of strength and ductility in titanium, metallurgists have developed alloys to allow for the retention of β phase in the final microstructure at room temperature. Through optimization of α and β phase, high strengths and ductility can be obtained. To control ductility and strength, titanium alloys include alloying elements to stabilize the α phase, the β phase, or both. Depending on volume fraction of the phases present, titanium alloys are classified as α alloys, α - β alloys or β alloys [2.35].

For α phase stabilization, alloying elements with atom/electron ratios below 4 [2.31] are added to titanium. Strong α stabilizers include aluminum, oxygen, carbon and nitrogen. Increasing the solute content with these elements in solid solution will effectively raise the β transus temperature, as illustrated in Figure 2.14 (a). In industry, aluminum is the main element used to stabilize α because it is the most commercially available metal that raises the β transus temperature while also having large solubility's in both the α and β phases.

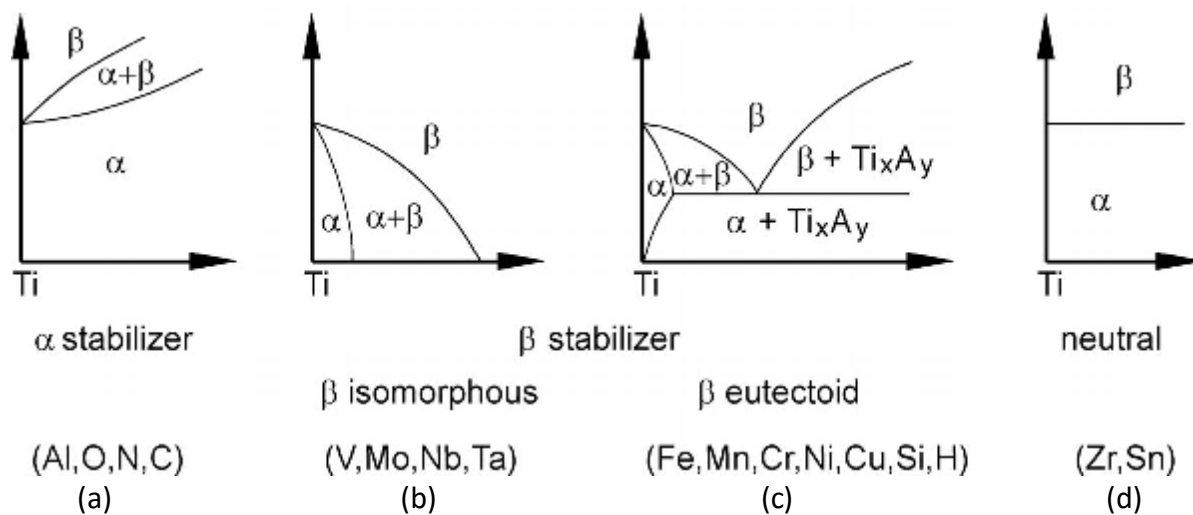


Figure 2.14: Phase diagrams for α stabilizing alloying elements (a), β stabilizing alloying elements (b,c) and neutral alloying elements (d) [2.36].

To stabilize the β phase, elements having atom/electron ratios above 4 are used. β phase stabilizers are either β isomorphous or β eutectoid. Common β isomorphous stabilizing elements include vanadium, molybdenum and niobium. Alloying titanium with β isomorphous elements allows for both α and β phase to be retained. Titanium α - β alloys are heat treatable and allow for a good mixture of strength and ductility to be obtained through post-processing.

Titanium alloys using β eutectoid stabilizing elements like chromium, iron and silicon are known to form intermetallic compounds. Most structural applications avoid using metals with β eutectoid elements, because the intermetallic compounds formed result in a reduction of fracture toughness and ductility [2.36]. They are however used in certain niche applications, where functionality at high service temperatures and low densities are required.

2.9 Ti6Al4V

Ti6Al4V is a binary α - β alloy which possesses an excellent combination of strength, toughness and corrosion resistance [2.37]. Ti6Al4V accounts for roughly 50% of all titanium production, as it is a frequent choice in the aerospace and biomedical industry due to its high specific strength and biocompatibility [2.37]. The excellent mechanical performance of Ti6Al4V is a result of aluminum and vanadium alloying elements allowing the microstructure of Ti6Al4V to retain both α and β phases at room temperature. The presence of both phases in the final microstructural composition has been seen in literature to yield high strength and ductility during mechanical testing. Depending on heat treatment and processing techniques, a variety of microstructural features and associated mechanical properties are attainable. Microstructural arrangements, common heat treatments and mechanical properties will all be discussed in subsequent sections.

2.10 Microstructure of Conventionally Processed Ti6Al4V

The microstructure of Ti6Al4V can evolve in different ways, depending on processing conditions. Mechanical deformation, heat treatments and cooling rates all play a role in determining the final microstructure of processed Ti6Al4V. Given that mechanical properties of Ti6Al4V are highly dependent on microstructure, it is important to strictly control processing conditions.

A common type of conventionally processed Ti6Al4V is the lamellar Ti6Al4V microstructure, sometimes also referred to as Widmanstätten microstructure. Lamellar microstructure is characterized by plates of α phase immersed within a matrix of β . A typical lamellar microstructure is seen in Figure 2.15 (a).

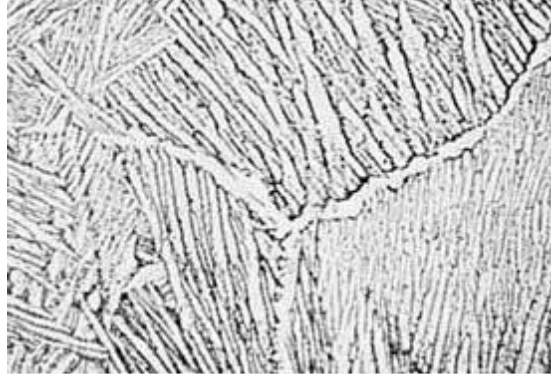


Figure 2.15: Ti6Al4V Lamellar Microstructure [2.39].

The progression of how lamellar microstructures are formed is shown in Figure 2.16. When Ti6Al4V is heated above the β transus temperature, only the β phase exists. After cooling to slightly below the β transus, tiny α plates begin to nucleate from prior β grain boundaries. As Ti6Al4V is further cooled, more of β is transformed to α , leading to the growth of α platelets. The cooling rate must be less than 1000 °C/minute, otherwise secondary meta-stable phases like α' and α'' will form. If α' and α'' phases are formed, they will need to be decomposed to α through additional heat treatments.

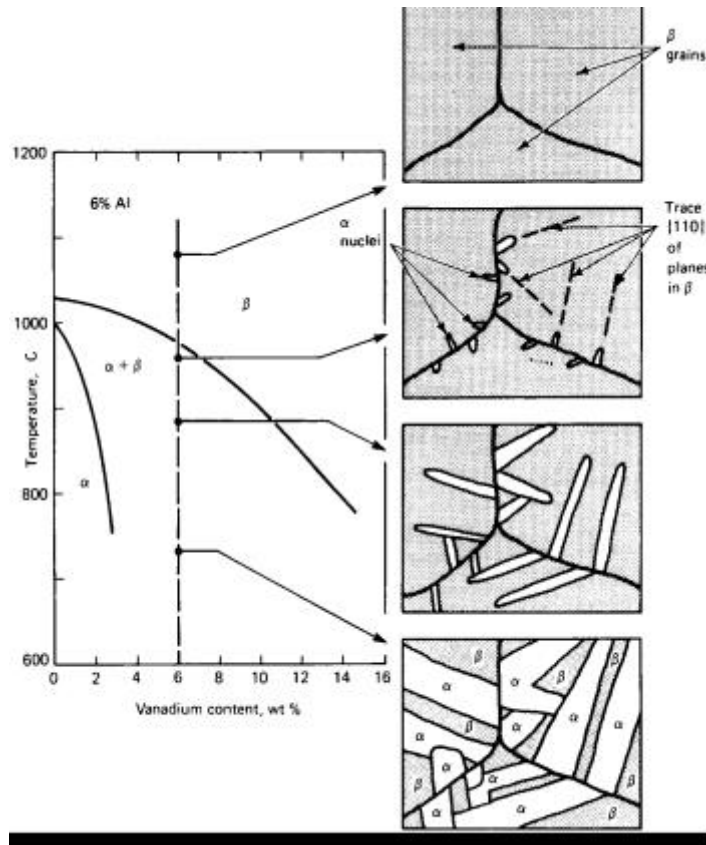


Figure 2.16: Development of Ti6Al4V Lamellar Microstructure [2.37].

2.11 SLM Processed Ti6Al4V Microstructure

Many works in literature have shown that a Ti6Al4V microstructure produced through SLM will have several unique characteristics, brought on by the process. This section will outline typical microstructures resulting from fabrication of samples with modern SLM machinery.

Characteristics inherent to the SLM process such as initial secondary α' phase and columnar grains will be described and their potential effect on performance will be discussed.

2.11.1 Columnar Grains

Ti6Al4V SLM studies using continuous Nd:YAG lasers have shown that columnar grains are a common characteristic in the microstructures of SLM fabricated samples [2.42,2.43,2.44,2.46,2.47]. Through SLM processing, columnar grains are frequently observed to elongate along prior- β grain boundaries, in the (100) build direction. These columnar grains are the result of the solidification process that starts at about 1660°C. It involves first the

solidification of the alloy into the crystallographic ordered state phase characterized by its body centered cubic (bcc) crystal structure. The base material or the previous layer of powder acts then as a preferential substrate on which solid growth is made possible. An epitaxially orientated type of growth will develop at the partially melted grains in the substrate and will strongly depend on its crystallographic effects such as existing grain orientations. Those with the easiest growth directions will then be preferred. In this case, the β phase grows preferentially with a solidification direction strongly dependent on the molten pool shape, where the general direction is perpendicular to the solid/liquid interface, following the maximum thermal gradient orientation. The columnar grains will grow aligned with the thermal gradient and may result in a curvature of the grains induced by the melt pool displacement [2.63].

A micrograph depicting columnar grains present in an SLM fabricated Ti6Al4V sample is shown in Figure 2.17.

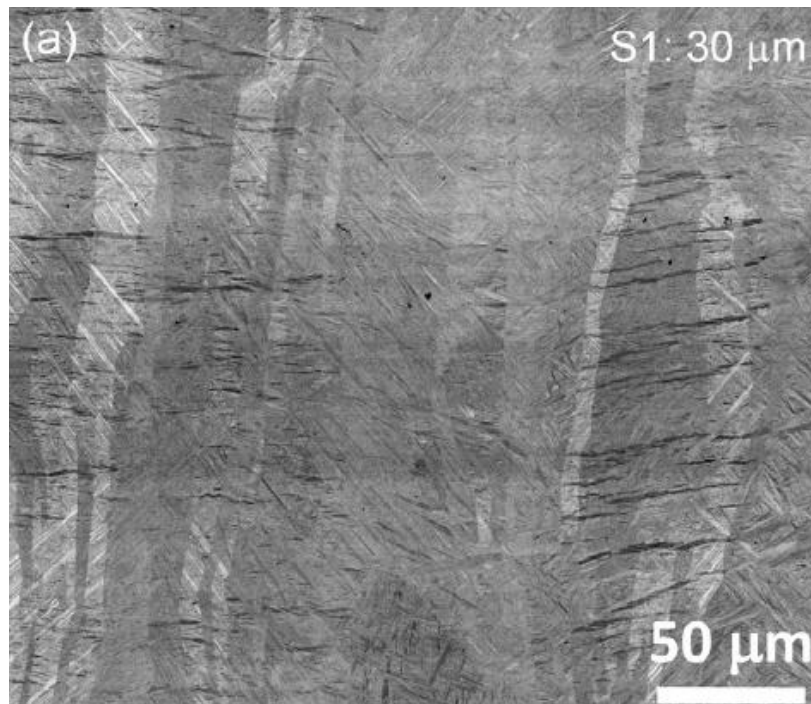


Figure 2.17: Columnar grains in SLM specimen [2.47].

With respect to mechanical properties, literature has shown that cracks have the propensity to propagate along columnar grains through fracture surface observation [2.49]. Some suggest that the presence of columnar grains in SLM samples may result in anisotropic mechanical

properties in the as-built condition. Depending on the loading with respect to columnar grain orientation, differences in ductility have been seen for horizontally and vertically built test specimens [2.43, 2.48].

2.11.2 Phase Composition

In current Ti6Al4V SLM literature, as-built SLM microstructure is composed entirely of the martensitic α' phase, with little of the α or β phases present [2.43,2.47,2.50]. This can be attributed to the high heating and cooling rates intrinsic to the SLM process. When powder is melted by laser interaction and upon solidification its cooling rate exceeds 1000 °C/min. These processing conditions satisfy requirements for martensitic formation, hence the resulting microstructure consists of α' martensite. Figure 2.18 shows an SEM image depicting the martensitic α' phase needles found in as-built SLM samples.

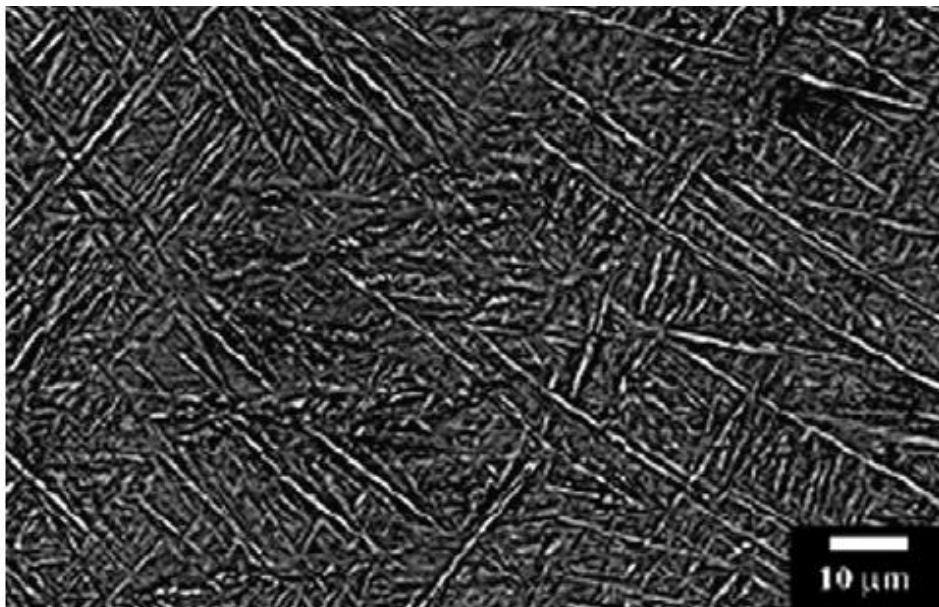


Figure 2.18: SEM image of α' martensite needles in as-built SLM condition [2.43].

Many studies have shown that a primarily α' microstructure results in low ductility [2.42, 2.43, 2.46, 2.51, 2.52]. By applying post-process heat treatments to decompose α' into microstructures consisting of α and β phases (i.e. lamellar microstructure), much improvement has been seen in ductility.

2.12 Defects in SLM of Ti6Al4V

With the integration of Nd:YAG laser systems in modern SLM machines, recent studies have shown that under optimal SLM machine conditions, densities above 99.5% are attainable for Ti6Al4V samples fabricated through SLM [2.42,2.43,2.44]. There is, however, a small amount of residual porosity left in the microstructure after processing. Some suggest that due to the apparent density of the powder bed (50-60%), small amounts of gas are entrapped in the material after solidification, which result in pores [2.45].

In Figure 2.19, two micrographs of the same sample demonstrate porosity after processing with SLM. Porosity can be seen to be randomized across the entire area of the sample. With higher magnification, these pores appear to be circular in shape and 50 μm in diameter.

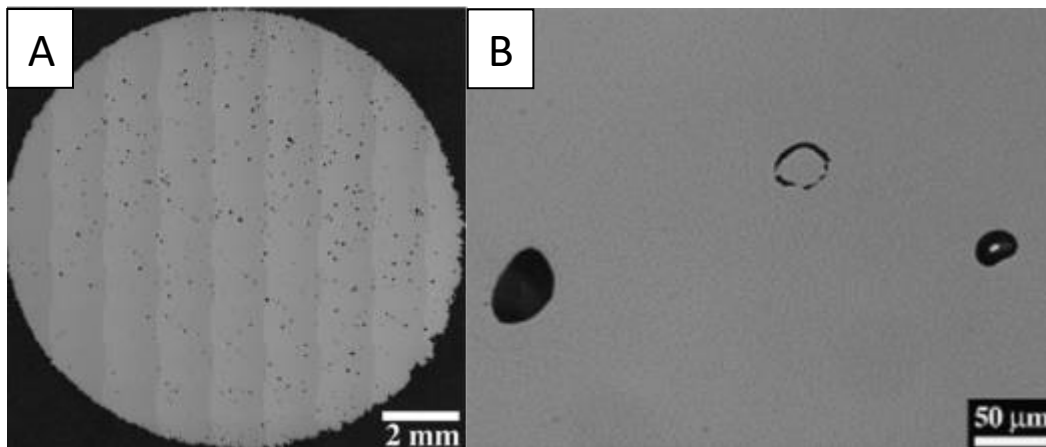


Figure 2.19 (a) and (b): Micrographs of SLM produced specimen, representing initial porosity [2.13].

Pores are detrimental to mechanical properties, as they act as stress concentrators during mechanical loading and have been seen to reduce fatigue life and final elongation of SLM parts. For that reason, one of the objectives of this study is to investigate porosity's influence on mechanical properties in SLM built parts.

2.13 Heat Treatment of Ti6Al4V

An advantage to titanium α - β alloys is that they are heat treatable and various properties can be optimized for specific application needs through heat treatment. In industry, heat

treatments are mainly applied to Ti6Al4V for internal stress relief and optimized mechanical properties [2.53]. Standard heat treatments for this alloy can be grouped into four categories:

- Stress Relief
- Annealing
- Solution Treating and Aging
- Hot-Isostatic-Pressing

It is important to note that for any heat treatment above 427 °C, a protective argon or vacuum environment must be used for titanium and titanium alloys [2.53]. At temperatures above 427 °C, oxygen from air will diffuse into solid-solution with titanium, forming an oxygen-enriched phase denoted alpha case [2.54]. Alpha case is extremely brittle and prone to micro-cracking, resulting in low ductility and fatigue properties. If alpha case is formed through heat treatment, it must be removed by machining or chemical milling before service.

2.13.1 Stress Relief

Stress relieving heat treatments are carried through primarily to relieve internal residual stresses built up during the processing of Ti6Al4V. Stress relief is not intended to modify the phase composition or mechanical properties of the alloy, although sometimes stress relief and annealing may coincide. Residual stresses are often detrimental to material integrity, frequently resulting in shape distortion and poor fatigue properties. In terms of build-up, residual stresses can be introduced in a variety of ways, including: non-uniform hot and cold working, asymmetrical machining, uneven cast cooling, welding and, as is the case in this study, rapid melting and re-solidification of metallic powder [2.53]. To fully relieve internal stresses, different combinations of temperature and time can be selected. Effective removal of internal stresses with lower temperatures require longer hold times, while higher temperatures can relieve stresses more quickly. A graph of residual stress versus time at various holding temperatures for Ti6Al4V can be seen in Figure 2.20

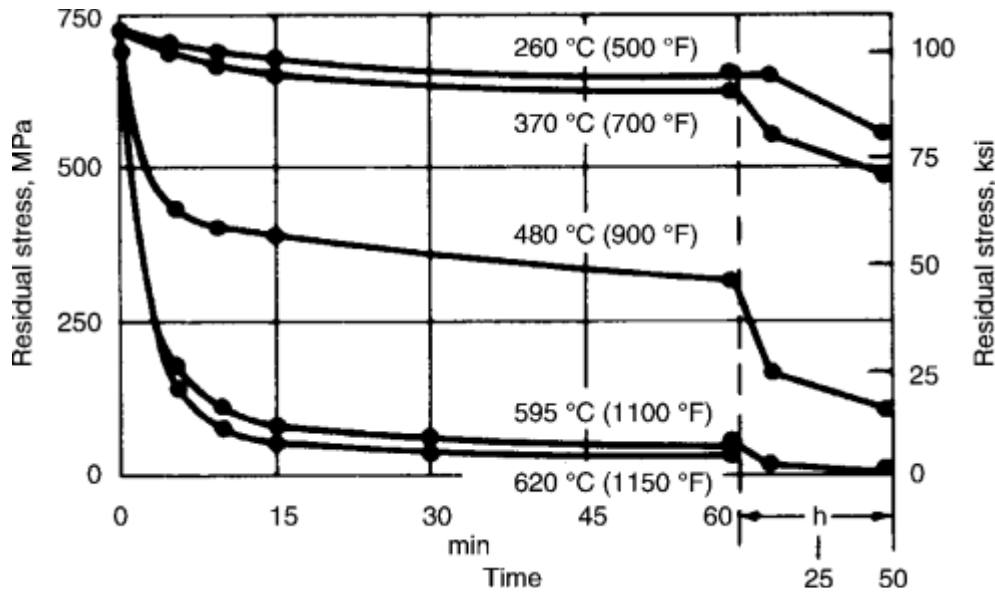


Figure 2.20: Relationship between time and amount of residual stress relief at various stress-relief anneal temperatures for Ti6Al4V alpha-beta alloy [2.55].

2.13.2 Annealing

Annealing is a generic term to describe heat treatments aimed at improving the toughness, ductility, thermal stability and creep resistance of Ti6Al4V [2.55]. Annealing heat treatments modify the phase composition and morphology of the microstructure, which in turn has influence on the mechanical properties of the material. Different annealing treatments exist, which can either involve heating to above or below the β transus temperature. The four main annealing heat treatments for Ti6Al4V include duplex, beta, recrystallization and mill anneals. A list of typical processing parameters used for these anneals, along with the microstructure produced can be seen in Table 2.2.

Mill annealing is performed at temperatures well below the β transus temperature (~ 700 °C), and is used to remove effects from prior hot and cold working on the metal. In addition, mill annealing will improve the overall toughness and ductility of the material. A duplex anneal involves a higher temperature anneal (~ 950 °C), just below the β transus temperature (980 °C). This high temperature anneal is followed by a standard mill anneal. Duplex annealing is an effective method to increase creep resistance and improve ductility.

Both recrystallization and beta annealing heat treatments are commonly used to significantly improve fracture toughness of Ti6Al4V. Beta annealing involves cooling from slightly above the β transus temperature, while recrystallization annealing remains below the transus temperature and involves hot working of the metal in the upper portion of the α - β region. Safety critical applications such as airframe components have in the past employed both recrystallization and beta annealing heat treatments, however recently recrystallization has been the more popular choice.

Table 2.2: Summary of annealing heat treatments for alpha-beta alloys, where T_{β} is the β -transus temperature of the particular alloy in question [2.53].

<u>Heat treatment designation</u>	<u>Heat treatment</u>	<u>Microstructure</u>
Duplex anneal	Solution treat at 50-75 °C below T_{β} , air cool and age for 2-8 h at 540-675 °C	Primary α , plus Widmanstatten α - β regions
Beta anneal	Solution treat at 15 °C above T_{β} , air cool and stabilize at 650-760 °C for 2 h	Widmanstatten α - β colony microstructure
Recrystallization anneal	925 °C for 4 h, cool at 50 °C/h to 760 °C, air cool	Equiaxed α with β at grain boundary triple points
Mill anneal	α - β hot work plus anneal at 705 °C for 30 min to several hours and air cool	Incompletely recrystallized α with a small volume fraction of small β particles

2.13.3 Solution Treating and Aging

Solution treating and aging (STA) heat treatments are used in α - β and β titanium alloys in order to obtain maximum strength levels. The working principal behind STA strengthening is that high volume fractions of β phase in the final composition result in high strengths.

STA heat treating can involve either heating slightly below the β transus temperature, in the α - β region, or slightly above, in the β region. Treatments which remain below the β transus temperature will possess high strengths and still retain adequate ductility. STA treatments that bring temperatures to above the β transus will have excellent strengths, however a significant

loss in ductility has been seen [2.56]. The trade-off in ductility for strength with increasing solution treatment temperature is shown in Table 2.3.

Table 2.3: Effect of solution treating temperature on tensile properties of Ti6Al4V barstock [2.57].

Solution-treating Temperature		Tensile Strength		Yield Strength		Elongation
C	F	MPa	ksi	MPa	ksi	%
845	1550	1025	149	980	142	18
870	1600	1060	154	985	143	17
900	1650	1095	159	995	144	16
925	1700	1110	161	1000	145	16
940	1725	1140	165	1055	153	16

In terms of procedure, STA heat treatments have three steps: solution treating, quenching and aging. First, Ti6Al4V is brought to the solution treating temperature (either slightly above or below the β transus), and held for 1 hour. Following the 1 hour hold time, a higher ratio of beta to alpha phase is present. To preserve the beta favoured phase partition, a water quench is executed following solution treatment. The rapid cooling provided by the water quench allows high amounts of β phase to remain in the microstructure at room temperature after cooling. After quenching, Ti6Al4V is aged for 4-8 hours, at temperatures ranging from 480-595 °C. The aging process will decompose any residual martensite and unstable β phase brought on by the quench, and effectively strengthen the material.

2.13.4 Hot-Isostatic-Pressing

Hot-Isostatic-Pressing (HIP) is a post-process heat and pressure treatment commonly employed to remove porosity from parts formed through casting or powder metallurgy (PM). HIP processing for Ti6Al4V is conducted in a heated, argon filled pressure vessel in the range of 895-955 °C and 10-30 ksi, for 2-4 hours [2.58]. Temperatures are kept below the β transus temperature so that HIP parts may retain good ductility.

In literature HIP has been seen to drastically improve fatigue property performance of cast and powder metallurgy parts. Improvement in fatigue strength and cycles to failure can be attributed to the removal of pores, which act as potential crack initiation sites during cyclic loading. Conversely, one drawback to the HIP process is that because of the high hold temperature, α platelets coarsen in the microstructure and a slight drop in overall tensile strength has been seen. Most often however, the benefit of better fatigue property performance far outweighs the minimal drop in tensile strength.

2.14 Mechanical Properties of SLMed Ti6Al4V

With the integration of AM as a legitimate manufacturing option in engineering design, it is of much importance to understand the capabilities and limitations of the SLM process for Ti6Al4V. From literature, most studies report that as-built SLM test specimens have excellent tensile strengths, often exceeding those of conventionally processed cast and wrought materials. High strengths of SLM specimens can be attributed to the fine microstructure obtained from rapid melting and cooling in the process. Although SLM parts exhibit high strength, one limitation of the process is that the final phase composition of the microstructure consists mostly of α' martensite, in the as-built condition [2.43,2.47]. Martensite is detrimental to mechanical properties, as specimens with martensitic microstructure have very low ductility when compared to wrought and heat treated Ti6Al4V. Table 2.4 displays a comprehensive list of mechanical properties from literature for as-built SLM parts. These SLM literature values are compared to the AMS 4911 standard for wrought annealed mill products [2.59] and the current ASTM standard for additive manufacturing of Ti6Al4V through powder bed fusion [2.60].

To improve the low ductility seen in as-built SLM products, it is common practice to apply post-processing treatments following fabrication of the part. Stress relief and annealing heat treatments have been seen to be effective in slightly improving ductility by decomposing α' into ultrafine lamellar mixtures of α and β [2.47]. In addition, Hot-Isostatic Pressing procedures have shown dramatic improvements in overall ductility and fatigue properties of SLM parts, as α' is decomposed to α in the process, porosity is eliminated and a higher volume fraction of β phase is present in the final microstructure [2.43].

Table 2.4: As-built mechanical properties of SLM Ti6Al4V in literature.

Reference	Condition	YS (MPa)	UTS (MPa)	Elongation (%)	Young's Modulus (GPa)	Vickers Hardness
Wrought AMS 4911 (Mill Annealed) [2.59]	-	920	1000	14	113.8	349
SLM Standard ASTM F2924 [2.60]	-	825	895	10	-	-
[2.43]	As-Built	1050	1225	5	-	-
[2.44]	As-Built	1125	1250	6	94	410
[2.62]	As-Built	1110	1267	7.28	109	-
[2.51]	As-Built	-	1000	5	-	379
[2.52]	As-Built	970	122	4	117	320
[2.42]	As-Built	1008	1080	1.6	-	-
[2.50]	As-Built	1075	1119	7.6	113	-

2.15 References

- [2.1] Levy, Gideon N. *The Role And Future Of The Laser Technology In The Additive Manufacturing Environment*. *Physics Procedia* 5 (2010): p. 65-80.
- [2.2] Gibson, I, D. W Rosen, and B Stucker. *Additive Manufacturing Technologies*. New York: Springer, 2010. p. 42-47
- [2.3] Gibson, I, D. W Rosen, and B Stucker. *Additive Manufacturing Technologies*. New York: Springer, 2010. p. 23
- [2.4] Qiu, C., N. Adkins, and M. Attallah. *Microstructure And Tensile Properties Of Selectively Laser-Melted And Of Hiped Laser-Melted Ti-6Al-4V*. *Materials Science and Engineering: A* 578 (2013): p. 230-239.
- [2.5] Vandenbroucke, B. and J.P. Kruth. *Selective Laser Melting Of Biocompatible Metals For Rapid Manufacturing Of Medical Parts*. *Rapid Prototyping Journal* 13.4 (2007): p. 196-203.
- [2.6] Löber, Lukas et al. *Selective Laser Melting Of A Beta-Solidifying Ti-6Al-4V Titanium Aluminide Alloy*. *Journal of Materials Processing Technology* 214.9 (2014): p. 1852-1860.
- [2.7] Meteyer, Simon et al. *Energy and Material Flow Analysis Of Binder-Jetting Additive Manufacturing Processes*. *Procedia CIRP* 15 (2014): p. 19-25.
- [2.8] Hermawan, H, D Ramdan, and J Djuansjah. *Metals For Biomedical Applications*. Biomedical Engineering - From Theory to Applications, 2011.
- [2.9] *MS&T'13 in Montreal: A Feast Of Additive Manufacturing Technology*. *Metal Powder Report* 69.1 (2014): p. 26-29.
- [2.10] Taminger, Karen M, and Robert A Hafley. *Electron Beam Freeform Fabrication (ebf3) for Cost Effective Near-net Shape Manufacturing*. Hampton, Va.: National Aeronautics and Space Administration, Langley Research Center, 2006.
- [2.11] Wauthle, R. et al. *Effects Of Build Orientation And Heat Treatment On The Microstructure And Mechanical Properties Of Selective Laser Melted Ti6Al4v Lattice Structures*. *Additive Manufacturing* 5 (2015): p. 77-84.
- [2.12] Simonelli, M., Y.Y. Tse, and C. Tuck. *Effect Of The Build Orientation On The Mechanical Properties And Fracture Modes Of SLM Ti-6Al-4V*. *Materials Science and Engineering: A* 616 (2014): p. 1-11.

- [2.13] EPRI, *Industry Segment Profile: Metal Powder Production*, Industry Segment Profile-SIC 33991, 2000. p. 1-38. Cost-effectiveness
- [2.14] Wohlers, Terry. *Past, Present and Future Of Rapid Prototyping*. IJPD 1.2 (2004): p. 147.
- [2.15] Leuders, S. et al. *On The Mechanical Behaviour Of Titanium Alloy Ti6Al4V Manufactured By Selective Laser Melting: Fatigue Resistance And Crack Growth Performance*. International Journal of Fatigue 48(2013): p. 300-307.
- [2.16] IndustrialLaser.com. *M2 Machine Specifications*. N.p., 2013. Web. 15 Apr. 2015.
- [2.17] Concept-laser.de. *News - Concept Laser'*. N.p., 2015. Web. 15 Apr. 2015.
- [2.18] Matilainen, Ville. *Benchmarking Of Laser Additive Manufacturing Process*. Bachelor's Thesis. Lappeenranta University of Technology, 2012.
- [2.19] Hengfeng Gu, Haijun Gong, Deepankar Pal, Khalid Rafi, Thomas Starr, Brent Stucker, *Influences of Energy Density on Porosity and Microstructure of Selective Laser Melted 17-4PH Stainless Steel*, Solid Freeform Fabrication Symposium, 2013, p. 474-489.
- [2.20] Spierings AB, G Levy. *Comparison of Density of Stainless Steel 316L Parts Produced with Selective Laser Melting Using Different Powder Grades*. Annual International Solid Freeform Fabrication Symposium, 2009.
- [2.21] Laoui, T., Wang, X., Childs, T.H.C., Kruth, J-P. and Froyen, L. , *Laser Penetration in a powder bed during selective laser sintering of metal powders, simulations versus experiments*, Proc. 11th Annual Solid Freeform Fabrication Symp., 2000, pg. 1.
- [2.22] Gibson, I, D. W Rosen, and B Stucker. *Additive Manufacturing Technologies*. New York: Springer, 2010. p. 123.
- [2.23] Elambasseril, Joe et al. *Influence of Process Parameters on Residual Stresses in Selective Laser Melting of Ti6Al4V Components*. 2012.
- [2.24] Yadroitsev, I., and I. Smurov. *Surface Morphology In Selective Laser Melting Of Metal Powders*. Physics Procedia 12 (2011): p. 264-270.
- [2.25] Yadroitsev, I. et al. *Strategy Of Manufacturing Components With Designed Internal Structure By Selective Laser Melting Of Metallic Powder*. Applied Surface Science 254.4 (2007): p. 980-983.

[2.26] Strano, Giovanni et al. *Surface Roughness Analysis, Modelling And Prediction In Selective Laser Melting*. Journal of Materials Processing Technology 213.4 (2013): p. 589-597. Surface rough 2

[2.27] Knowles, C. *Residual Stress Measurement And Structural Integrity Evaluation Of SLM Ti-6Al-4V*. M. Sc. University of Cape Town, 2012: p. 51.

[2.28] Aboulkhair, N.. et al. *Reducing Porosity In AlSi10Mg Parts Processed By Selective Laser Melting*. Additive Manufacturing 1-4 (2014): p. 77-86.

[2.29] Gibson, I, D. W Rosen, and B Stucker. *Additive Manufacturing Technologies*. New York: Springer, 2010. p. 133.

[2.30] Gibson, I, D. W Rosen, and B Stucker. *Additive Manufacturing Technologies*. New York: Springer, 2010. p. 2.

[2.31] Udomphol, T. *Titanium And Its Alloys*. Suranaree University of Technology. N.p., 2007. Web. 6 Apr. 2015.

[2.32] Hermawan, H, D Ramdan, and J Djuansjah. *Metals For Biomedical Applications*. Biomedical Engineering - From Theory to Applications, 2011.

[2.33] Lütjering, G, and J. C Williams. *Titanium*. Berlin: Springer, 2007. p. 16.

[2.34] Donachie, M. *Titanium: A Technical Guide*. Materials Park, Ohio: ASM International, 2010. p. 2.

[2.35] Donachie, M. *Titanium: A Technical Guide*. Materials Park, Ohio: ASM International, 2010. p. 13.

[2.36] Lütjering, G, and J. C Williams. *Titanium*. Berlin: Springer, 2007. p. 24.

[2.37] Donachie, M. *Titanium: A Technical Guide*. Materials Park, Ohio: ASM International, 2010. p. 22.

[2.38] Donachie, M. *Titanium: A Technical Guide*. Materials Park, Ohio: ASM International, 2010. p. 20.

[2.39] Donachie, M. *Titanium: A Technical Guide*. Materials Park, Ohio: ASM International, 2010. p. 17

[2.40] Lütjering, G, and J. C Williams. *Titanium*. Berlin: Springer, 2007. p. 204.

[2.41] Lütjering, G, and J. C Williams. *Titanium*. Berlin: Springer, 2007. p. 211

[2.42] Leuders, S. et al. *On The Mechanical Behaviour Of Titanium Alloy TiAl6V4 Manufactured By Selective Laser Melting: Fatigue Resistance And Crack Growth Performance*. International Journal of Fatigue 48(2013): p. 300-307.

[2.43] Qiu, C., N. Adkins, and M. Attallah. *Microstructure And Tensile Properties Of Selectively Laser-Melted And Of Hiped Laser-Melted Ti-6Al-4V*. Materials Science and Engineering: A 578 (2013): p. 230-239.

[2.44] Vandenbroucke, B. and J.P. Kruth. *Selective Laser Melting Of Biocompatible Metals For Rapid Manufacturing Of Medical Parts*. Rapid Prototyping Journal 13.4 (2007): p. 196-203.

[2.45] Aboulkhair, N.. et al. *Reducing Porosity In Alsi10mg Parts Processed By Selective Laser Melting*. Additive Manufacturing 1-4 (2014): p. 77-86.

[2.46] Simonelli, M., Y. Tse, and C. Tuck. *The Formation Of $\alpha + \beta$ Microstructure In As-Fabricated Selective Laser Melting Of Ti-6Al-4V*. Journal of Materials Research 29.17 (2014): p. 2028-2035.

[2.47] Xu, W. et al. *Additive Manufacturing Of Strong And Ductile Ti-6Al-4V By Selective Laser Melting Via In Situ Martensite Decomposition*. Acta Materialia 85 (2015): p. 74-84.

[2.48] Wauthle, R. et al. *Effects Of Build Orientation And Heat Treatment On The Microstructure And Mechanical Properties Of Selective Laser Melted Ti6al4v Lattice Structures*. Additive Manufacturing 5 (2015): p. 77-84.

[2.49] Antonysamy, A. *Microstructure, Texture And Mechanical Property Evolution During Additive Manufacturing Of Ti6al4v Alloy For Aerospace Applications*. Ph.D. University of Manchester, 2012: p. 280.

[2.50] Simonelli, M., Y.Y. Tse, and C. Tuck. *Effect Of The Build Orientation On The Mechanical Properties And Fracture Modes Of SLM Ti-6Al-4V*. Materials Science and Engineering: A 616 (2014): p. 1-11.

[2.51] Knowles, C. *Residual Stress Measurement And Structural Integrity Evaluation Of SLM Ti-6Al-4V*. M. Sc. University of Cape Town, 2012: p. 168

[2.52] Aziz, I. *Microstructure and Mechanical Properties of TiAl6V4 produced by Selective Laser Sintering of Prealloyed Powders*. M. Eng. University of Wikato, 2010: p. 81

[2.53] Donachie, M. *Titanium: A Technical Guide*. Materials Park, Ohio: ASM International, 2010. p. 55

- [2.54] Mutombo, K., P. Russouw, and G. Govender. *Chemically Milled Alpha-Case Layer From Ti6Al4V Alloy Investment Cast. MSF 690* (2011): p. 477-480.
- [2.55] Donachie, M. *Titanium: A Technical Guide*. Materials Park, Ohio: ASM International, 2010. p. 57
- [2.56] Donachie, M. *Titanium: A Technical Guide*. Materials Park, Ohio: ASM International, 2010. p. 58
- [2.57] Donachie, M. *Titanium: A Technical Guide*. Materials Park, Ohio: ASM International, 2010. p. 59
- [2.58] Donachie, M. *Titanium: A Technical Guide*. Materials Park, Ohio: ASM International, 2010. p. 63
- [2.59] SAE AMS 4911, *Titanium Alloy, Sheet, Strip, and Plate, 6Al - 4V, Annealed*, SAE Aerospace.
- [2.60] ASTM F2924-14, *Standard Specification for Additive Manufacturing Titanium-6 Aluminum-4 Vanadium with Powder Bed Fusion*, ASTM International, West Conshohocken, PA, 2014, www.astm.org
- [2.61] Lütjering, G, and J. C Williams. *Titanium*. Berlin: Springer, 2007. p. 186.
- [2.62] Vrancken, Bey et al. *Heat Treatment Of Ti6Al4V Produced by Selective Laser Melting: Microstructure And Mechanical Properties*. *Journal of Alloys and Compounds* 541 (2012): p. 177-185.
- [2.63] David, S.A. and Vitek, J.M. *Correlation between Solidification Parameters and Weld Microstructure*. *International Materials Reviews*, Volume 34, Number 5, (1989): p. 213-245.
- [2.64] Kruth J P, Badrossamay M, Yasa E, et al. *Part and Material Properties in Selective Laser Melting of Metals*. *Proceedings of the 16th International Symposium on Electromachining*, 2010

Chapter 3: Experimental Methodology

3.1 Introduction

This chapter will first describe the different processing and post-processing techniques chosen to enhance the mechanical properties of as-built Ti6Al4V samples in this study. The post-processing techniques aim to maximize the mechanical properties which were then compared with wrought benchmarks, as well as the ASTM F2924 standard for powder bed fusion of Ti6Al4V. Afterwards, the methods and equipment used to examine material and mechanical properties will be described in detail.

3.2 SLM Machine

An M2 Cusing machine, manufactured by Concept Laser in Germany, was used to fabricate all samples discussed in this project. The machine can be seen in Figure 3.1. The M2 Cusing machine melts metallic powder through use of a diode-pumped, 200W Nd:YAG laser. The laser has a wavelength of 1070 nm, and is capable of scanning parts at speeds up to 7 meters per second. Parts can be built up to 250x250 mm in the x-y plane and 280 mm in height. Build rates for the machine range from 5-20 cm³/hour, depending on machine parameters selected. A list of technical details can be seen in Table 3.1.



Figure 3.1: M2 Cusing SLM machine by Concept Laser used to fabricate samples in this study.

A key feature of this machine resides in the possibility to work with reactive metals such as titanium and aluminum. Under the M2 system, powder is at all times sealed within an inert

atmosphere, through use of a glove-box designed for powder and part handling. The glove-box system is effective in both minimizing oxidation of the powder, and adding to the safety of powder handling.

Table 3.1: List of technical data for M2 Cusing SLM machine.

Technical Details	
Build envelope	250x250x280mm (x,y,z)
Layer thickness	20 -80 μm
Production speed	2-20 cm^3/h
Laser system	Fibre laser 200 W (cw), optional 400 W (cw)
Max. scanning speed	7 m/s
Focus diameter	50-200 μm
Reference clamping system	EROWA, System 3R
Connected loads	Power consumption 7.4 W, Power supply AC 400V, 32A
Inert gas supply	2 gas connections provided
Inert gas consumption	< 1 m^3/h
Dimensions	2440x1630x2354 mm (WDXH)
Weight	2000 kg
Operating conditions	15-35 $^{\circ}\text{C}$

3.3 Part Orientation

Samples were built in the X,Z and 45° directions to gather a comprehensive set of comparative data. The effects of build orientations on mechanical properties and microstructural characteristics will be discussed in Chapter 4. The layout can be seen in Figure 3.2.

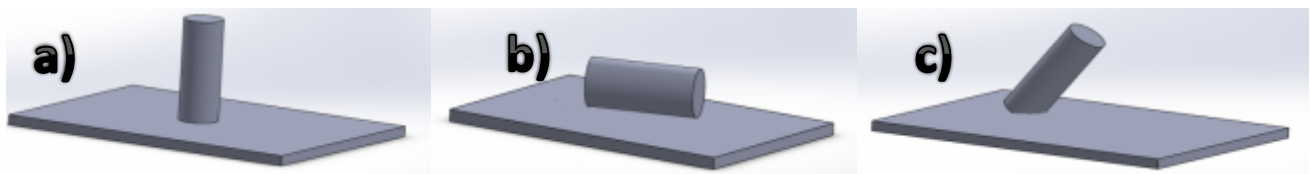


Figure 3.2: Example of samples built in (a) Z, (b) X and (c) 45° orientations on build plate.

3.4 Post-Processing Treatments

To optimize mechanical properties, three post-process procedures were selected for treating as-built samples. These include (1) a stress relief heat treatment recommended by the Society of Automotive Engineers (SAE AMS2801), (2) an annealing heat treatment recommended again by SAE (AMS2801), and (3) a hot iso-static pressing heat and pressure treatment recommended by ASTM standard F2924 for powder bed fusion of Ti-6Al-V4.

3.5 Sample Fabrication and Post-Processing

Mechanical properties in this thesis were obtained using rounded tensile coupons. Coupon dimensions were built according to the ASTM E8M-04 standard for tensile testing. The gauge length and diameters of the coupons were 30 and 6 mm, respectively. ASTM E8M-04 can be seen in Figure 3.3.

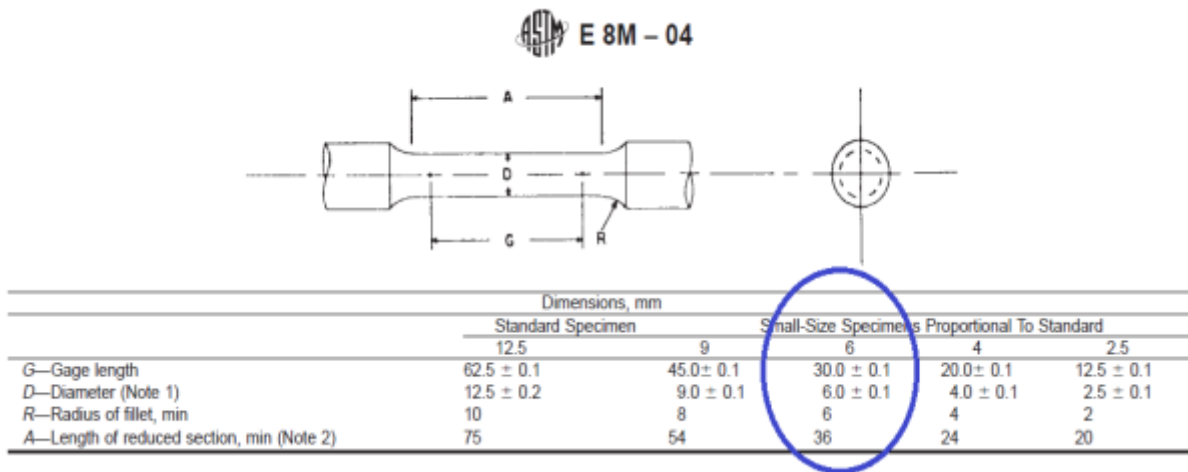


Figure 3.3: ASTM E8M –04 dimensions used to fabricated tensile coupons.

SLM machine build parameters were selected by taking the highest density yielding parameter set from the three tested sets. Samples were constructed in three separate builds, due to space limitations on the build plate. Each build contained samples of the same build orientation (X,Z and 45°). These as-built batches are seen in Figure 3.4.

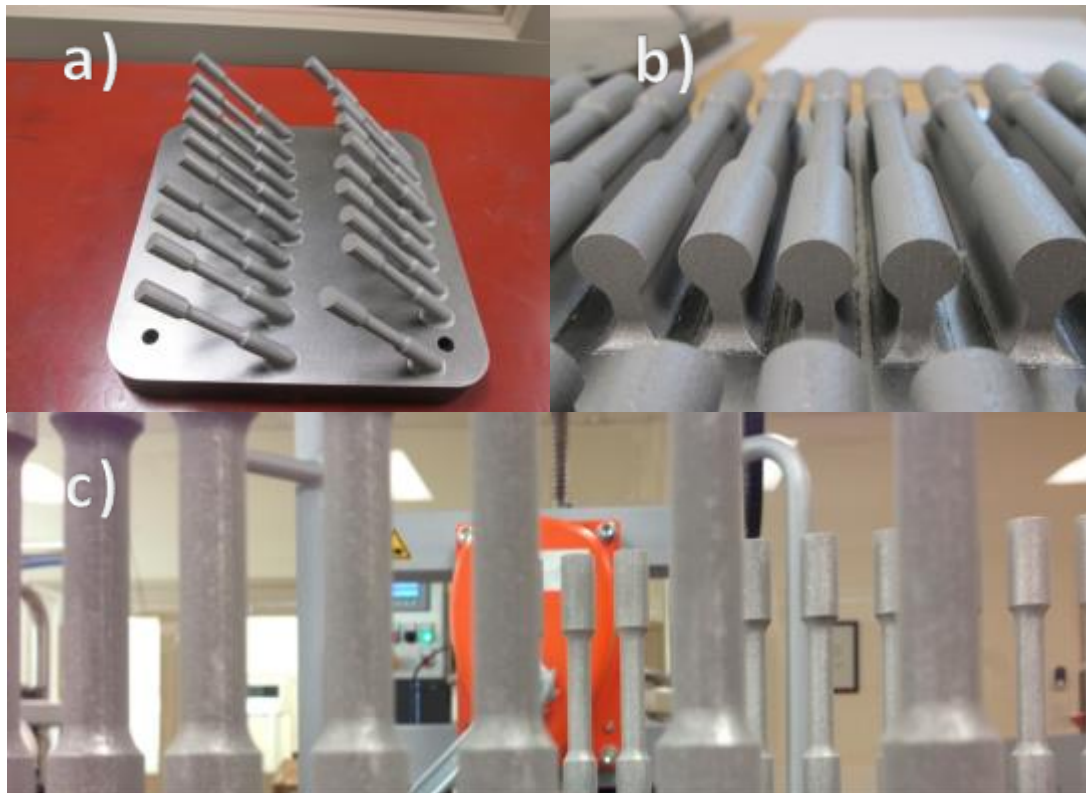


Figure 3.4: As-built tensile coupons built in the 45° (a), x (b) and z (c) orientations.

After the initial build process, samples were cut from the build plate through use of a band-saw and further post-processed to the conditions listed in Table 4.2. A test matrix of the samples can be seen in Table 3.4.

Table 3.2: Test Matrix of samples

Post-Process Condition	x	45°	Z
Build + Stress Relief (1)	5 samples	5 samples	5 samples
Build + Annealing (2)	5 samples	5 samples	5 samples
Build + HIP (3)	5 samples	5 samples	5 samples

In order to prevent oxidation of the samples during heat treatment, stress relief procedures were conducted in an argon furnace. The furnace selected was an N41/H Nabertherm furnace, capable of reaching temperatures up to 1280 °C in a protective argon gas atmosphere. For the HIP procedure, an American Isostatic HIP furnace was used. The maximum temperature and pressure attainable on the HIP furnace were 1400 °C and 30 ksi, respectively. Mill annealed samples were outsourced to the heat treatment company Thermetco for processing in a vacuum furnace. Pictures of the furnaces can be seen in Figure 3.5.

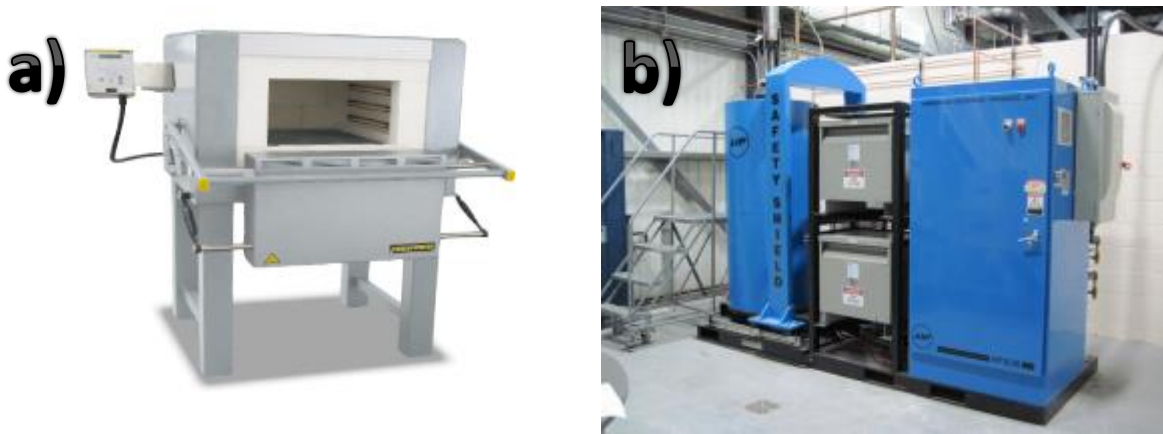


Figure 3.5: (a) Nabertherm argon furnace and (b) American Isostatic HIP furnace used in post-processing of the as-built samples.

3.6 Tensile Testing of Coupons

All tensile tests were performed on a 55 000 lb-force MTS manufactured load frame, equipped with a calibrated load cell and extensometer. The samples were tested in accordance with all ASTM E8M-04 standards for tensile testing. Strain was measured through both cross-head displacement and an extensometer attachment. The strain rate used was 0.03 millimeters per second. Samples were threaded to minimize potential of slip during testing.

From the data collected from tensile testing, the following mechanical properties were determined:

- i) Yield Strength – The stress at which plastic deformation begins to occur.
- ii) Ultimate Tensile Strength – The highest stress attained before fracture.
- iii) Elongation to fracture – The elongation of the sample at fracture point.
- iv) Young’s Modulus – The stress to strain slope during elastic deformation.
- v) Area % Reduction – The final deformed diameter of the gauge compared to initial.

3.7 Porosity Measurement

Porosity levels were found through optical microscopy thresholding on a Clemex microscope. Sections from tensile samples were taken and then polished to a mirror-like finish by following the steps in Table 3.5.

Table 3.3: Grinding and polishing procedure for sample preparation.

Step	Grinding Surface	Time Held (minutes)
1	240 grit SiC grinding paper	3
2	400 grit SiC grinding paper	3
3	600 grit SiC grinding paper	3
4	1200 grit SiC grinding paper	3
5	Colloidal SiC vibromet	120

3.8 Microstructural Analysis

Sample microstructure was observed through both optical and scanning electron microscopy. A Clemex microscope was used for optical micrographs, while a Hitachi SU3500 scanning electron microscope (SEM) was used for back scatter electron (BSE) images of the tensile fracture surfaces. Samples were prepared for optical microstructural analysis by using the grinding and polishing procedure outlined in Table 3.5. This was followed by etching the samples with a hydrofluoric acid (HF) solution containing 2% HF and 98% distilled water for 20 seconds. The Hitachi SU3500 SEM was also used to conduct an electron back scatter diffraction (EBSD) analysis, which was used to determine crystal orientation and texture of test specimens. X-ray diffraction analysis was conducted on a D8 Discovery XRD apparatus to determine volume fraction of phases in microstructure.

Chapter 4: Structure and Property Relationships associated with Selective Laser Melting of Ti6Al4V

Preface

Structure and Property Relationships associated with Selective Laser Melting of Ti6Al4V is a comprehensive work which includes all experimental procedures and expected results outlined in Chapter 4. This paper is intended to be published in a scientific journal during the 2016 year. Results for machine parameter optimization, microstructure analysis, mechanical properties and texture analysis are presented in detail and will be discussed in this chapter. The citation of this article is as follows:

J. Mezzetta, J. Milligan, J. Danovitch, N. Chekir, L. Nguyen and M. Brochu. *Structure and Property Relationships Associated with Selective Laser Melting of Ti6Al4V*. Article intended for publication. 2016.

Abstract

To implement additive manufacturing techniques like selective laser melting (SLM) into aerospace and biomedical manufacturing practice, it is imperative to ensure that the mechanical behaviour and performance of selective laser melted Ti6Al4V parts are understood and reliable, and if possible, match that of wrought material, especially for safety critical applications. This work investigates the relationships between static mechanical properties of Ti6Al4V manufactured through SLM and post-process heat treatments. It was found that properties exceeding some wrought AMS specs were obtained after application of a hot-isostatic-press (HIP). Within the realm of the tensile properties, the yield and ultimate strength values were found statistically similar with respect to built orientation for a given heat treatment. However, a mismatch in ductility was found for the HIP samples, where a lower value was observed for samples built in the X direction.

Key words:

Selective Laser Melting
Titanium
Heat Treatment
Mechanical Properties
Microstructure
Hot-Isostatic-Pressing

4.1 Introduction

Selective Laser Melting (SLM), one of the key additive manufacturing (AM) processes, is a manufacturing route with research roots dating back to the late 1980's [4.1]. As opposed to subtractive manufacturing where material removal occurs, the main premise behind SLM is that components are built in an additive manner involving a layer-by-layer fusion and solidification of fine metallic powder, displayed as a powder bed, using a high power laser beam. The laser raster path creates the part profiles. Ultimately, through continuous stacking and bonding of layers, net-shape components can be fabricated in a single process. This disruptive advantage allows for the fabrication of complex shapes with intricate external and internal features, impossible to manufacture using conventional techniques.

The state-of-the-art SLM technology now routinely permits the fabrication of Ti6Al4V parts exceeding 99.5% in density [4.2,4.3,4.4,4.13]. The remnant porosity is associated with either gas entrapment occurring during the process or incomplete melting/filling of the cavity by the melt pool [4.5]. With respect to the associated mechanical properties, as-built Ti6Al4V SLM parts exhibit high strengths and low ductility when compared to conventional wrought Ti6Al4V. The accepted explanation relates to the extremely high cooling rates exhibited in SLM favouring the development of the strong-but-brittle martensitic α' phase present in the as-built microstructure [4.2,4.4,4.6]. To reduce the mismatch between the mechanical properties of SLM and wrought, previous works in literature have attempted to increase ductility through application of post-SLM heat treatment. In general, SLM heat treatments are either processed in high pressure (hot isostatic press - HIP), atmospheric (inert gas) or vacuum furnaces. Inert gas or vacuum furnaces are capable at decomposing martensitic α' into the more ductile α and β phases [4.11,4.16], however these SLM parts would still possess porosity remaining from the initial SLM process. Despite the softening in microstructure, the resultant ductility is ultimately lower than wrought parts. On the other hand, HIP heat treatments are capable of closing residual porosity remaining from initial SLM builds, while successfully decomposing α' into α and β [4, 6]. Closed porosity, combined with phase transformations, allow HIP processed samples to achieve mechanical properties that are comparable to wrought

material.

While it is known that phase composition and size, and porosity are the two largest factors dictating mechanical performance. Literature on martensitic decomposition via conventional Solution Treatment and Aging (STA) suggests to heat treat in the 480-595 °C range for 4-8 hours [4.23], while some in the AM community have demonstrated martensitic decomposition while using furnace temperatures as low as 400 °C [4.15]. SLM studies have shown the α' platelets present in as-built SLM parts range from 0.3-0.6 μm in width [4.15,4.19,4.22]. Through application of heat treatment, α' plates can transform to α and coarsen to somewhere in the 1-2.5 μm range, depending on the specific heating cycle [4.2,4.4,4.6,4.11,4.20,4.21]. This is significant when looking at mechanical properties, as the strength of Ti6Al4V is highly dependent on α width. In one Ti6Al4V study looking at the correlation between mechanical properties and microstructural characteristics, a model comparing α plate width to yield strength was made from 0.5-1.5 μm [4.24]. The pronounced effect of α width was highlighted, as the 0.5 μm to 1.5 μm coarsening resulted in a linear decrease of strength from 830 to 760 MPa.

Another critical factor influencing the Ti6Al4V SLM parts is the presence of columnar grains [4.2,4.3,4.4,4.6,4.15,4.18]. Due to rapid heating and melting of thin powder layers in SLM, β grains grow epitaxially and result in elongated grains of β . After rapid solidification, β is transformed to α' martensite, however artifacts from the prior- β grains remain. As a result, the final microstructure consists of variants of α' immersed within elongated prior- β grains. Some in literature suggest that the presence of columnar grains is directly responsible for anisotropy seen in the mechanical properties of SLM parts [4.2,4.4,4.18]. For this reason, further investigation is needed to characterize the microstructure of SLM samples and observe the influence microstructure has on mechanical properties.

In this study, tensile coupons were built in the x, z and 45° orientations to determine any anisotropy in mechanical properties. Crystallographic texture analysis and fracture surface

analysis were performed on all three orientations to determine texture's effect on mechanical properties. The same samples were also given three furnace heat treatments, both HIP and non-HIP, to observe the influence of phase composition on mechanical properties. These results combined with in depth fracture surface analysis was performed to provide additional insight in the mechanical properties of Ti-6Al-4V parts.

4.2 Experimental Methodology

The AM samples were fabricated using a Concept Laser M2 Cusing and spherical Ti6Al4V ELI grade powder supplied by the machine manufacturer. The morphology of the spherical powder particles is depicted in Figure 4.1. The particle size distribution, specified to range between 20-50 microns, was confirmed using a Horiba Laser Diffraction Particle Analyzer. The chemical composition of the powder from the supplier data sheet is shown in Table 1. Oxygen being the critical impurity, its content was confirmed by inductively coupled plasma (ICP) analysis and yielded 0.11 wt%, i.e. within the allowable ELI grade tolerance.

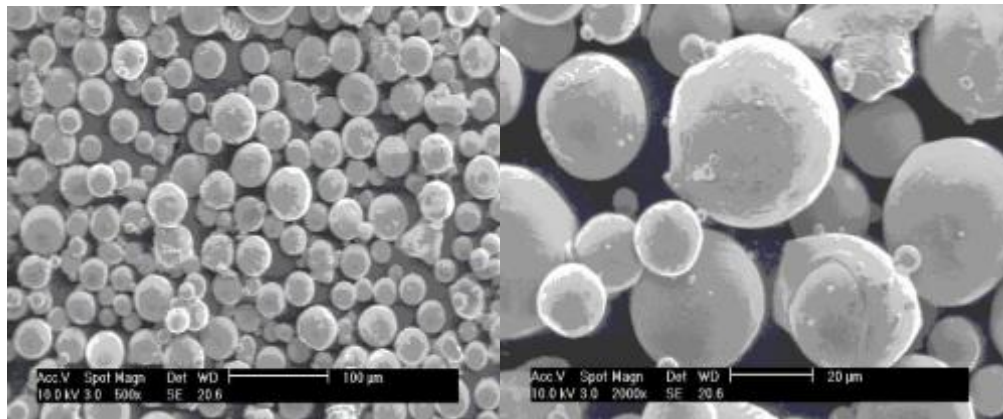


Figure 4.1: SEM images of gas atomized Ti6Al4V powder particles

Table 4.1: Ti6Al4V Alloy Composition; data provided by the supplier.

Alloy	Impurity Limits, wt % max				
	N	C	H	Fe	O
AMS 4907 ELI Ti-6Al-4V	0.05	0.08	0.012	0.25	0.13

Round tensile samples were fabricated in accordance with the ASTM E8-04 standard, and these samples were used for both microstructural and mechanical property testing. Tensile samples were built in the X, Z, and 45° orientations to determine the effect of build orientation on properties. The samples were prepared using a Concept Laser M2 Cusing SLM system, using the standard building parameters for Ti-6Al-4V. Upon fabrication, all samples were stress relieved according to AMS 2801 standard [4.9], to prevent geometrical deformation of the samples upon removal from the base plate. Selected samples for the three build directions were then further annealed according to AMS 2801 standard [4.9]. Finally, samples from the three build directions were subjected to HIP using the processing parameters specified in the ASTM F2924 standard [4.7]. After heat treatment, the samples were CNC machined to size, to eliminate surface artifacts from processing and heat treatment. A total of 45 samples were tested to assess the parameters in this test matrix: there were five samples per condition and the values reported are the average of each 5-sample set.

Typical metallographic procedures, including a final polishing on colloidal silica using a Vibromet, were used to prepare the different surfaces for microstructural observation. Density assessment was performed by optical microscopy using a Clemex microscope followed by image analysis (Clemex Professional Edition) on polished cross sections. The microstructural examination of the phases was done on etched samples in a solution containing 2% hydrofluoric acid (HF) and 98% distilled water for 20 seconds. Scanning electron microscopy (SEM) was done on a Hitachi SU-3500. In addition to the surface analysis, the SEM was used to conduct electron back-scattered diffraction (EBSD) analysis using HKL Channel 5 software for data processing to determine crystallographic orientation and texture of the different specimens. X-ray diffraction analysis was conducted on a D8 Discovery XRD apparatus to determine volume fraction of phases in the microstructures.

Tensile testing and Vickers microhardness were used to assess the mechanical properties. From tensile testing, mechanical properties such as yield strength (YS), ultimate tensile strength (UTS) and elongation were found using a 55 kip MTS load frame equipped with a calibrated load cell and

extensometer. Microhardness was determined through a Clark Microhardness Indenter. Indentations were performed at 100g load and the reported values are an average of 20 indents.

4.3 Results and Discussion

4.3.1 Evaluation of Density

Table 4.2 shows the evolution of the porosity, measured by image analysis, as a function of the various heat treatment imposed on the SLM part. In the as-built condition, the image analysis indicated a residual pore volume fraction of $0.39 \pm 0.10\%$. These pores developed due to entrapped gas within the powder bed and are consistent with previously described pore formation in fully melted and 99.5%+ dense SLM specimens [4.3, 4.4]. Table 4.2 also indicates the porosity level measured in the stress relieved and mill annealed conditions, which both have similar residual porosity than in the as-built condition ($0.40 \pm 0.32\%$ and $0.39 \pm 0.31\%$, respectively), while the HIP process was successful in eliminating all porosity to at least beyond the resolution of the optical microscope.

Table 4.2: SLM Part Porosity after Experimental Heat Treatments.

	Porosity (%)
As-built	0.39 ± 0.10
Stress relief	0.40 ± 0.32
Mill anneal	0.39 ± 0.31
HIP	<0.01

4.3.2 Microstructure

Similar to previous studies, columnar grains were observed in all samples, independently of the build orientation [4.2,4.4,4.5,4.11,4.15,4.17]. Figure 4.2 shows the difference in columnar grain orientation observed for the tensile samples built in the X, 45° and Z conditions, respectively, with the tensile test loading direction specified on each micrograph. Rather than extending through the entire sample height, columnar grains break after growing a few mm. This leads to the stacking of columnar grains on top of one another. Image analysis indicated that the grain

dimensions were 1.55 ± 1 mm in length and 0.20 ± 0.08 mm in width, and the results were independent of the built orientation. These columnar grains are the result of the solidification process that starts at about 1660°C . It involves first the solidification of the alloy into the crystallographic ordered state phase characterized by its body centered cubic (bcc) crystal structure. The base material or the previous layer of powder acts then as a preferential substrate on which solid growth is made possible. An epitaxially orientated type of growth will develop at the partially melted grains in the substrate and will strongly depend on its crystallographic effects such as existing grain orientations. Those with the easiest growth directions will then be preferred. In this case, the β phase grows preferentially with a solidification direction strongly dependent on the molten pool shape, where the general direction is perpendicular to the solid/liquid interface, following the maximum thermal gradient orientation. The columnar grains will grow aligned with the thermal gradient and may result in a curvature of the grains induced by the melt pool displacement [4.10].

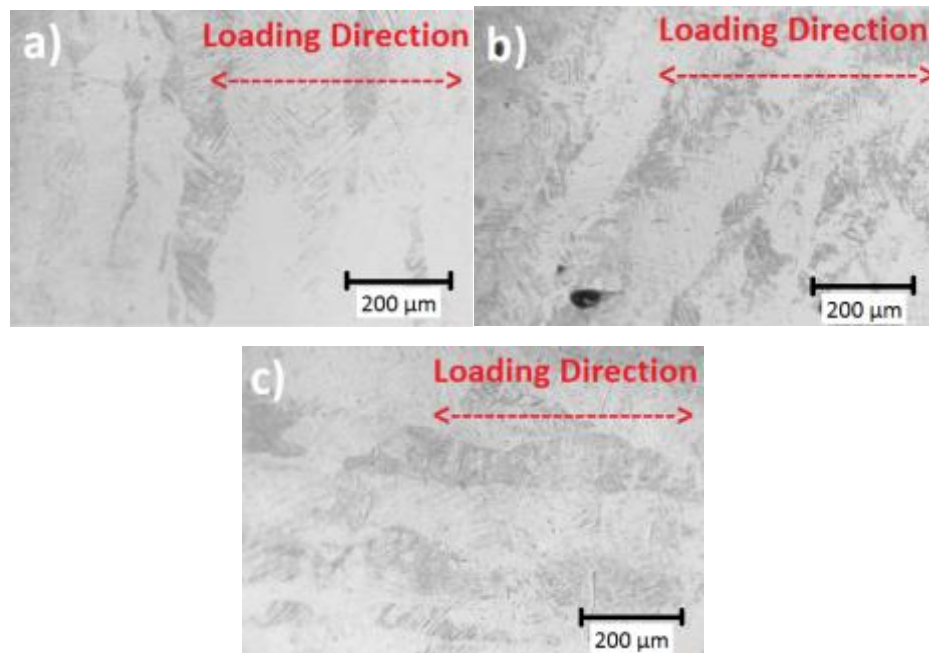


Figure 4.2: Optical micrograph depicting columnar grains in (a) X-built tensile samples, b) 45° -built tensile samples and (c) Z-built tensile samples, with loading direction for tensile testing specified.

Upon subsequent fast cooling, a new solid phase transformation occurs at the beta transus temperature which is 999 ± 28 °C for this alloy [4.9]. Depending on the cooling rate, this transformation involves a change in crystallography of the bcc phase into the hexagonal close packed (hcp) phase or martensitic α' phase. As expected, and in agreement with other works [4.2,4.4], the as-built microstructure was entirely composed of the martensitic structure. The burgers relationships shown in Equations 1 and 2 shows the preferential crystallographic orientation relationship between the BCC and HCP phases. This phase transformation in Ti6Al4V is known to transform into 12 hexagonal variants: lamellae developing at the prior-beta grain boundaries and growth primarily controlled by the previously mentioned crystallographic considerations.

$$(110)_{\beta} \parallel (0002)_{\alpha} \quad 1$$

$$[\bar{1}\bar{1}1]_{\beta} \parallel [11\bar{2}0]_{\alpha} \quad 2$$

The decomposition of the martensitic phase is critical to recover ductility. The optical micrographs presented in Figure 4.3a, 4.3b and 4.3c show the microstructure for the three post processing heat treatment conditions, respectively. Figure 4.3a depicts the microstructure of the samples in the stress relief condition, which appear to consist mostly of α' martensitic needles. These needles are 10.5 ± 2.7 μm in length and 1.0 ± 0.6 μm in width. Figure 4.3d shows the corresponding XRD pattern for this structure, where the pattern indicates only α/α' , with no β phase present. From this, it can be seen that the stress relief heat treatment is insufficient in fully transforming the microstructure from $\alpha' \rightarrow \alpha + \beta$. Other studies have also confirmed that post-process heat treatments near 600°C have been insufficient in transforming any α to β [4.2,4.4]. Figure 4.3b presents the microstructure obtained after the annealed heat treatment. With the higher temperature anneal, the microstructure coarsened significantly with respect to the stress relief condition. The average α/α' plate/needle was found to be 12.5 ± 3.5 μm in length, and 2.0 ± 0.8 μm in width. The corresponding XRD spectra are presented in Figure 4.3e

and also suggest the lack of development of the β phase during this heat treatment. In literature, heat treatment near 800°C have lacked β phase as well [4.6]. The alpha peaks see a shift to the left for 2-Theta, which others have proposed in literature is due to a transformation from $\alpha' \rightarrow \alpha$ [4.4]. With respect to the samples exposed to the HIP cycle, the obtained microstructure presented in Figure 4.3c consisted of a lamellar composite of α and β , with fractions of β appearing at the boundaries of α plates. Alpha plates in the HIP condition possess the largest average dimensions, having lengths of $12.8 \pm 4 \mu\text{m}$ and widths of $3.2 \pm 0.6 \mu\text{m}$. The XRD spectra for this microstructure is presented in Figure 4.3f and confirms the presence of the β phase, quantified to 3% volume fraction through intensity ratios of crystal structures. HIP processed samples were performed approximately 40 °C under the β transus temperature, and it is possible that the added pressure may have altered the phase transformation temperature, resulting in β phase nucleating below the β transus temperature . It is also possible that β phase nucleated exclusively due to the elevated temperatures, as studies have shown non-pressurized furnaces are capable of producing β below the transus temperature [4.2].The presence of β phase post-HIP agrees with conventional casting requiring HIP procedures.[4.25].

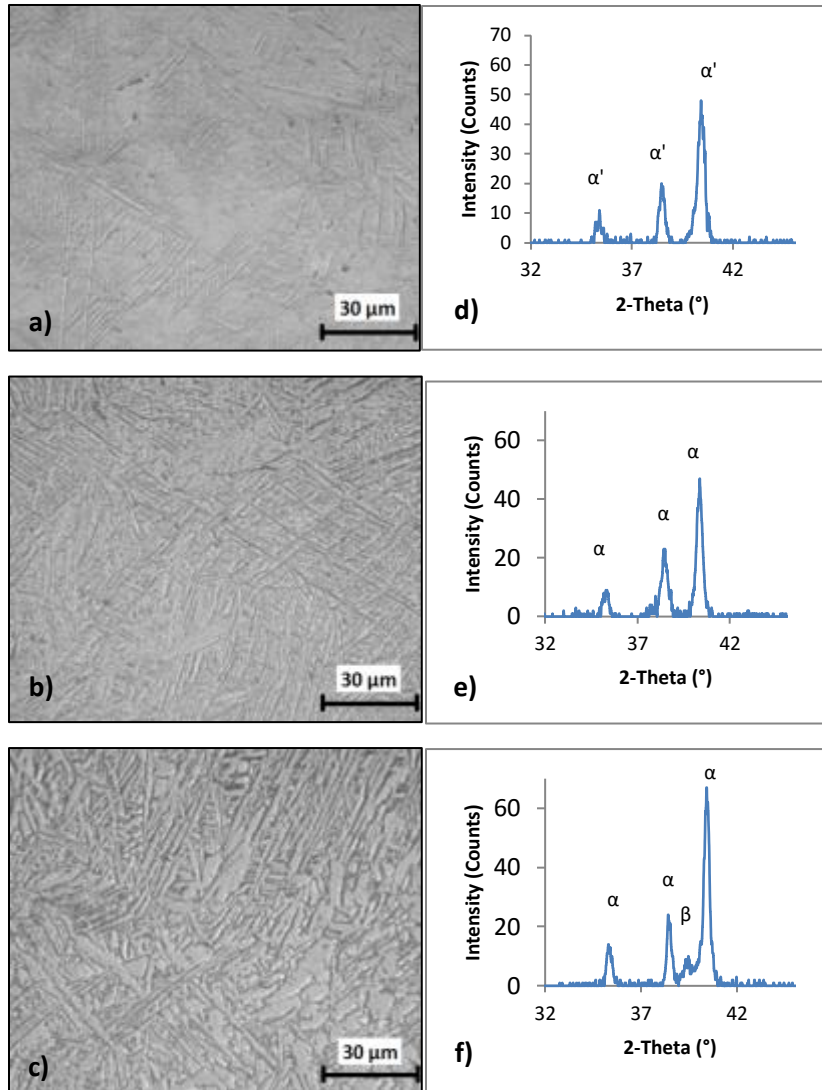


Figure 4.3: Microstructures in the (a) stress relief, (b) mill anneal and (c) HIP conditions, respectively, with corresponding XRD spectra (d,e,f)

To complement the investigation of the microstructure, EBSD was performed to investigate if preferential orientation of the alpha platelet developed. Figures 4.4 and 4.5 show results from EBSD texture analysis of the α -phase for HIP tensile samples built in the z-direction and in the x-direction respectively, taken from the columnar grain face in each case. Visual analysis of the inverse pole figure (IPF) maps suggest that the α crystals are randomly oriented throughout the sample, with similar orientations delimited by the boundaries of the α colonies. The pole figures and corresponding inverse pole figures generated from this data support this claim, indicating

only very weak texture if any. It has been suggested that the α'/α phase in SLM Ti6Al4V has weak texture due to the high number of variants that precipitate within each columnar β grain [4.2]. Thus, no correlation between the mechanical properties and the crystallographic texture of the Ti- α phase is expected.

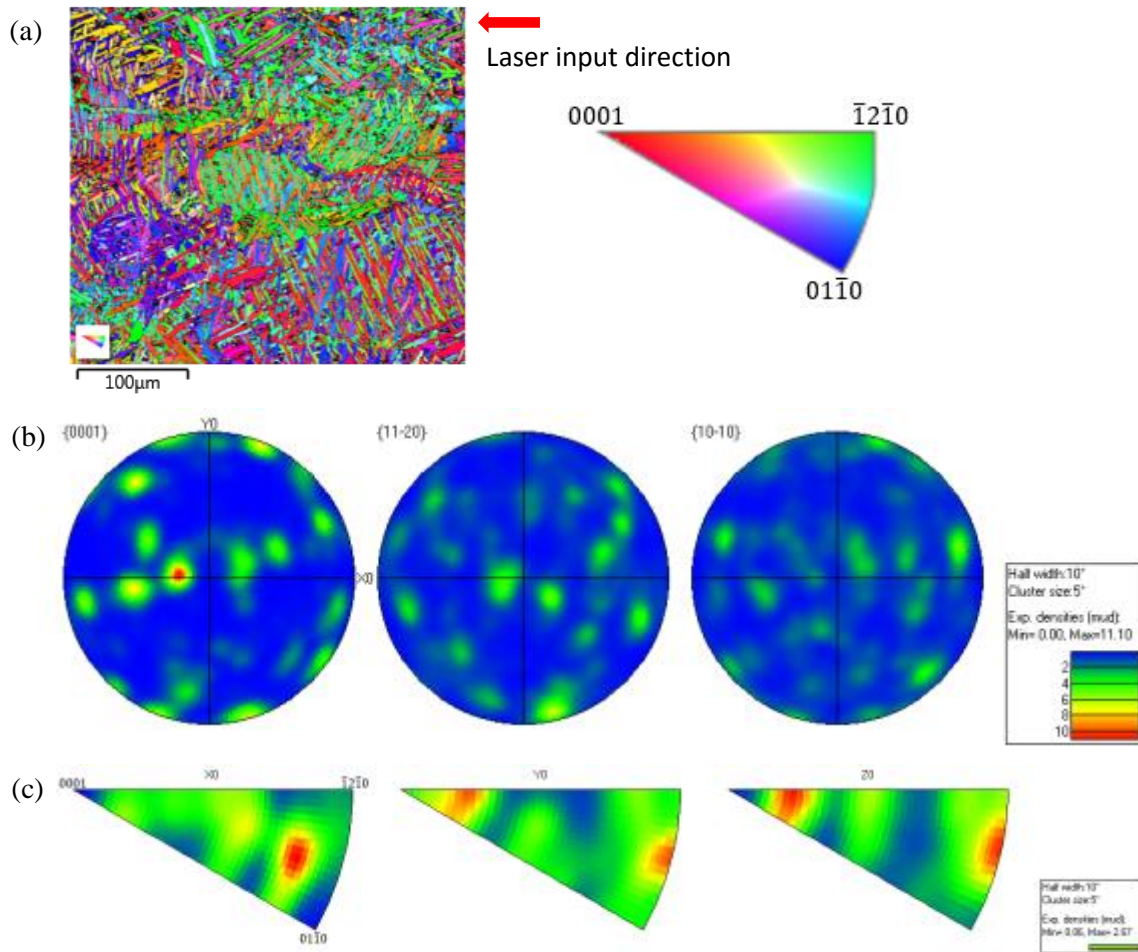


Figure 4.4: EBSD texture analysis conducted on the Ti- α phase of a side view of a tensile sample built in the z-direction, with the direction of pull oriented in the horizontal axis, showing (a) IPF map normal to plane, (b) pole figures for three main crystal orientations in the HCP system, and (c) corresponding IPFs.

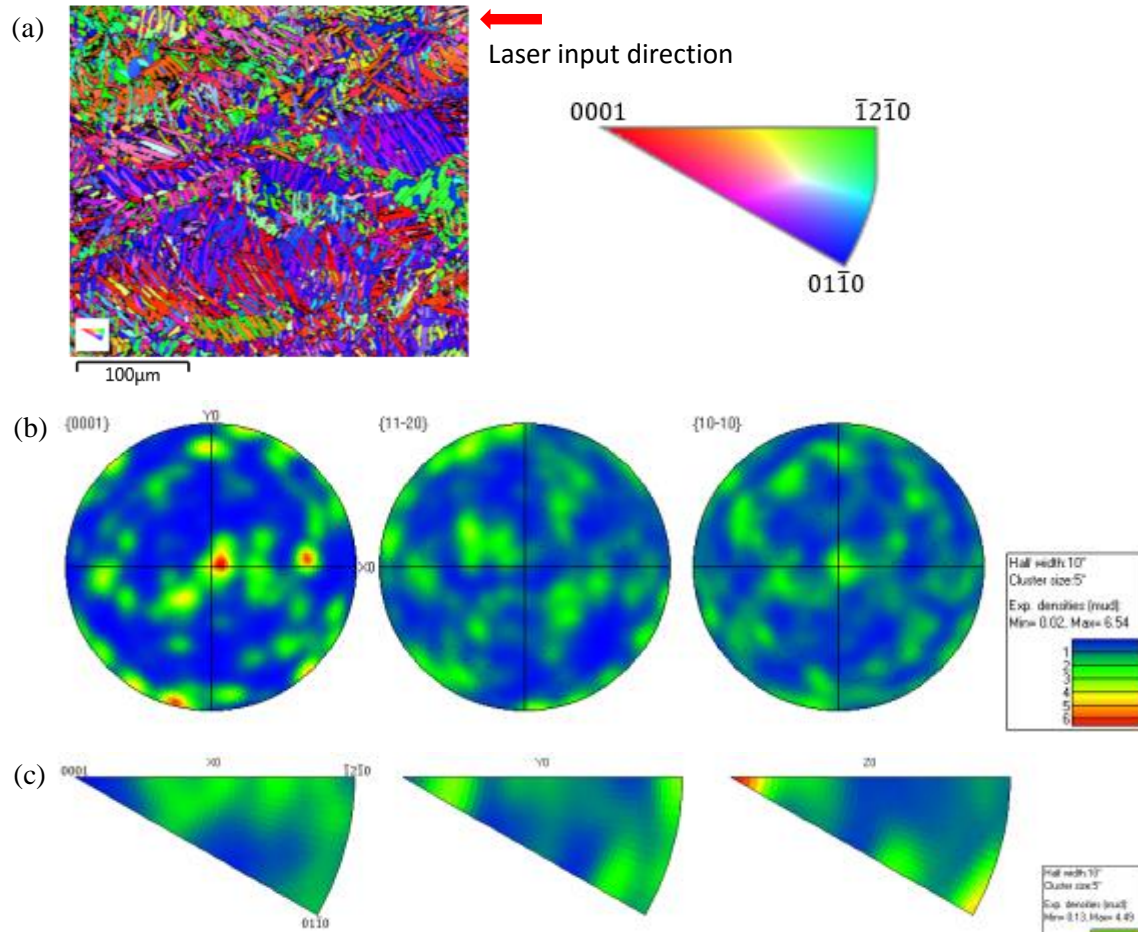


Figure 4.5: EBSD texture analysis conducted on the Ti- α phase of a top view of a tensile sample built in the x-direction, with the direction of pull oriented in the axis normal, showing (a) IPF map normal to plane, (b) pole figures for three main crystal orientations in the HCP system, and (c) corresponding IPFs.

4.3.3 Mechanical Properties

A summary of the Vickers microhardness values for three processing conditions and build directions are presented in Table 4.3. Upon examination of the results, it can be seen that the stress relief condition possessed the highest hardness values. This is most likely due to the martensitic microstructure seen in the previous section, where the microstructure was dominated by ultra-fine needles. Mill annealed samples saw a softening of the microstructure, which can be attributed to the coarsening of α/α' platelets, along with a partial transformation of $\alpha' \rightarrow \alpha$. A further increase in softness was seen for the HIP samples. This may be caused by the 3% volume fraction of β , which is a softer phase, as well as the further coarsening of the α platelets. The as-built Vickers Hardness values are similar to other values found in the literature for similar conditions [4.3, 4.12].

Mechanical results extracted from the tensile testing are displayed in Figure 4.6 and Figure 4.7, along with other values found in literature. Stress relieved tensile samples had the highest YS and UTS of the three processing conditions. Compared to literature, these values are on the high end of the spectrum. This is probably due to high cooling rates induced on the M2 Cusing machine, resulting in very small α' platelets. Conversely, ductility for the stress relieved samples were very low. This high strength, low ductility combination can most likely be explained by the presence of α' martensite in the microstructure after stress relieving. When compared to the ASTM F2924 standard for additive manufacturing of Ti6Al4V [4.7], and the AMS 4911 standard for mill annealed wrought Ti6Al4V material [4.8], all samples in the stress relief condition exceeded strength requirements. On the other hand, the final elongation obtained was considerably short of the 10% final elongation requirement of ASTM F2924.

Table 4.3: Vickers hardness for experimental samples

Vickers Hardness (HV)			
Post-Process Condition	X	Z	45°
Stress Relief	418 ±10	424 ± 9	414 ± 8
Mill Anneal	395 ± 6	394 ± 6	388 ± 12
HIP	374 ± 5	379 ± 5	373 ± 9

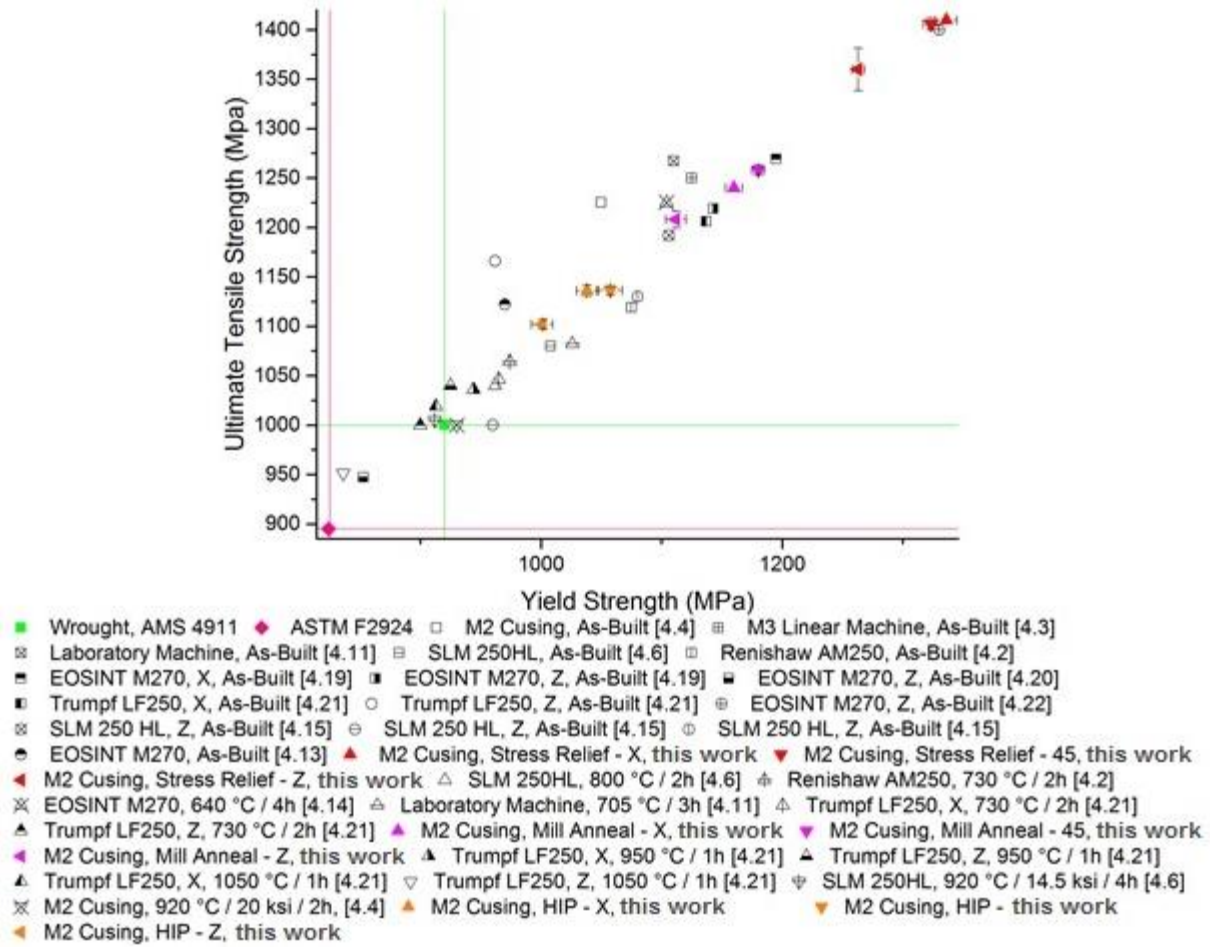


Figure 4.6: Ultimate Tensile Strength versus Yield Strength for Stress Relief, Mill Anneal and HIP conditions in X, 45° and Z build directions compared to existing values from literature.

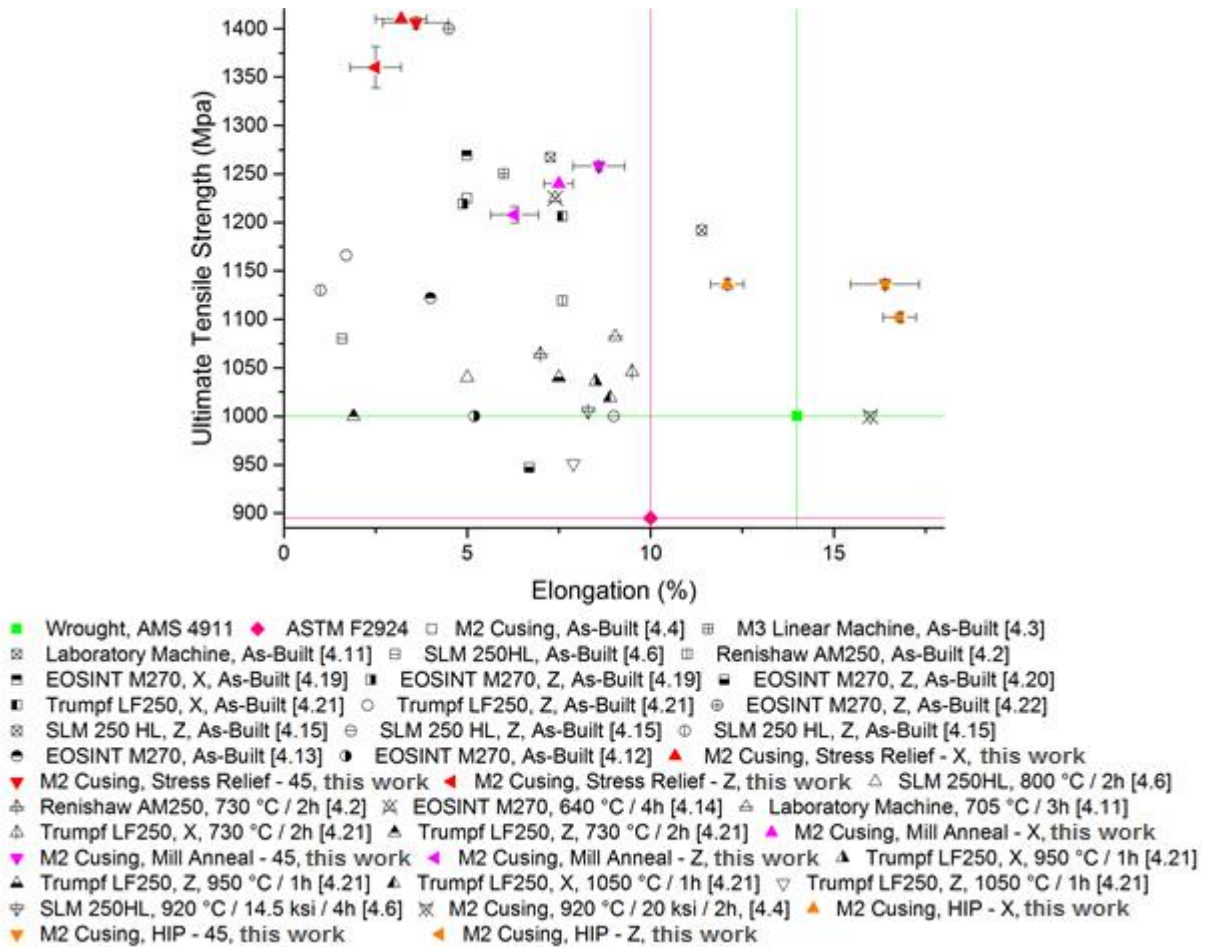


Figure 4.7: Ultimate Tensile Strength versus Final Elongation for Stress Relief, Mill Anneal and HIP conditions in X, 45° and Z build directions compared to existing values from literature.

In the case of mill annealing, there was an increase in ductility when compared to the stress relief condition, albeit with a trade-off in strength. Final elongation values were on average much higher than the stress relieved condition. Compared to ASTM and AMS standards, all mill annealed samples exceeded strength requirements, but as with the stress relieved condition, fell short of the 10% final elongation requirement. This softening of the mechanical properties is mostly likely due to the coarser α platelets, along with the transformation of $\alpha' \rightarrow \alpha$. Within the detection limit of XRD, the spectra shown in Figure 4.3 suggests that mill annealing has a very similar phase composition to stress relieving.

The HIP samples also experienced a reduction in strength but conversely; an increase in ductility was seen. In terms of strength, all samples exceeded the ASM and ASTM values. All final elongation values for HIP samples satisfied the 10% ASTM standard requirement for all build orientations and even exceeded those of wrought Ti6Al4V (14%) in the case of Z and 45° built HIP samples. A combination of porosity closure, further coarsening of the α lathes and a higher volume fraction of β phase is thought to be responsible for this dramatic increase in ductility.

As shown, a mismatch in strength and final elongation values is observed between the various build orientations and heat treatment. Samples built in the X and 45° orientations exhibited similar strengths for all post-processing conditions (i.e., overlapping of error bars); however, all Z samples were seen to be of less strength. Owing to the idea that each sample within one heat treatment condition should have similar phase volume fraction and that the EBSD results showed little to no preferential texture of the α crystals, this disparity in mechanical properties is most likely associated with the columnar grains that are oriented differently with respect to the loading direction, based on build direction [4.4, 4.18]. Property anisotropy will be further discussed in the fracturography section which follows.

4.3.4 Fracture Surfaces

The analysis on post-test fracture surfaces reveals that fracture modes vary significantly for samples built in different orientations (i.e. Z versus X). An overview of the fracture path is shown in Figure 4.8 for HIPed X and Z samples.

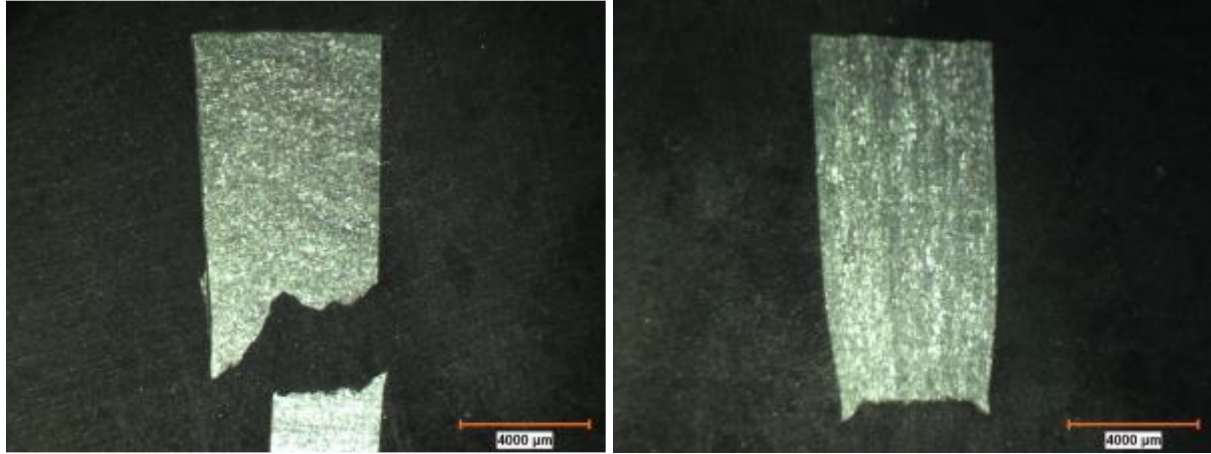


Figure 4.8: Fracture of HIPed X-oriented sample (a), versus HIPed Z-oriented sample (b).

It can be observed that the Z sample exhibits classic cup and cone fracture associated with high elongation, while the X sample undergoes a tumultuous diagonal fracture path.

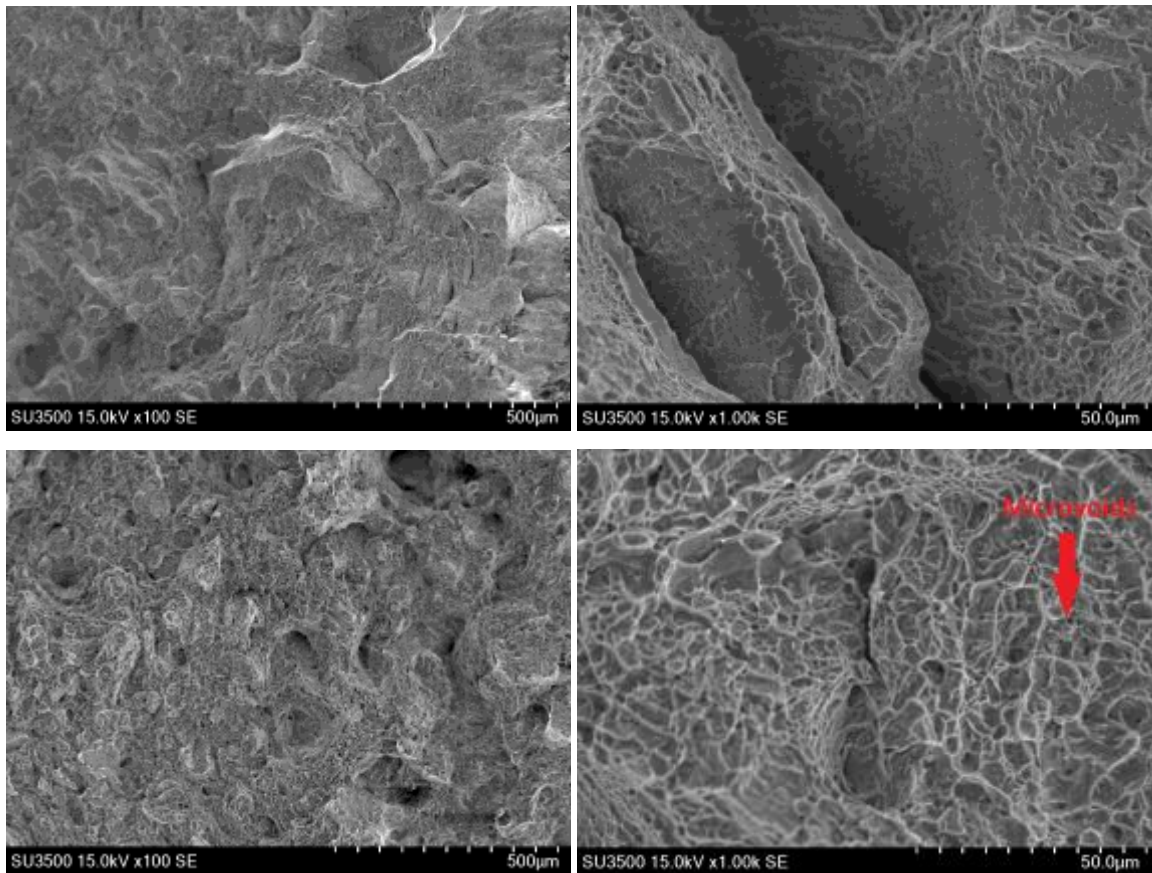


Figure 4.9: SEM images for fracture surface of HIP X sample (a,c) and HIP Z sample (b,d).

SEM images of the fracture surfaces in Figure 4.9 show that, similar to other fractography studies [4.2,4.4], all fracture surfaces demonstrate a certain degree of intergranular fracture. These surfaces are characterized by large, planar terraces which are formed from cracks initiating and propagating along prior- β or α grains. There is however a mixed fracture mode present for HIPed samples built in the Z direction, as ductile microvoids can be seen in Figure 4.9 (d). The mixed fracture mode may explain the increased ductility of Z built samples when compared to X (which experiences only mostly intergranular fracture).

A possible reason for the mixed fracture mode (ductile and brittle) seen in Z samples could be due to prior- β columnar grain orientation with respect to loading direction. Columnar grains were observed to be parallel to the load direction in Z built samples and perpendicular to the load direction in X built samples. Since colonies of α platelets are restricted to grow within prior- β grain boundaries, colonies of α are free to extend further down a columnar grain (approximately 0.5-3mm), than across a columnar grain (0.1-0.3mm). For example, in Z samples, the load is being applied down the columnar grain. This may result in increased slip distances on average across α colonies in Z samples than X samples. Considering the inverse relationship between slip distance and yield strength, anisotropy in mechanical properties could possibly be seen for samples of different build orientation owing to slip distance dependence on build orientation.

4.3.5 Conclusions

The main focus of this work was to observe the static mechanical behaviour of Ti6Al4V fabricated through SLM, and develop relationships between mechanical properties and microstructure. To optimize mechanical properties, a series of post-SLM heat treatments were given to as-built SLM tensile coupons. These coupons were fabricated in X, 45° and Z build directions to investigate multi-directional mechanical performance.

After experimentation, it was determined that only samples post-processed with HIP had properties approaching those of wrought Ti6Al4V. Stress relief and mill anneal post-SLM heat

treatments met strength benchmarks, however both of these conditions exhibited relatively low ductility. From microstructural analysis, the low elongation values in these cases can most likely be attributed to a still martensitic α' microstructure, along with a scattering of remaining porosity. Unlike the stress relief and mill anneal heat treatments, HIP resulted in a full closure of porosity, and was also successful in transforming the initial martensitic microstructure into a fully lamellar arrangement of $\alpha + \beta$. These are thought to be the reasons for the remarkable increase in ductility for HIP samples.

In all post-processing conditions, anisotropy in mechanical properties was observed between the three different build orientations. Samples built in the X direction yielded the highest strengths, samples built in the Z had the lowest, while 45° had strengths between the two.

Conversely, X built samples demonstrated lowered ductility when compared to Z and 45° samples. This is thought to be because of columnar grain arrangement with respect to loading direction and varying slip distances due to differences in α colony sizes for the X, 45° and Z build directions.

From visual analysis of the Euler and inverse pole figures generated by EBSD, no strong α texture was seen in either the X or Z built samples. From this, it is difficult to correlate between the mechanical properties and the crystallographic texture of the Ti- α phase from the data produced in this experiment.

4.7 References

- [4.1] Levy, Gideon N. *The Role And Future Of The Laser Technology In The Additive Manufacturing Environment*. *Physics Procedia* 5 (2010): p. 65-80.
- [4.2] Simonelli, M., Y.Y. Tse, and C. Tuck. *Effect Of The Build Orientation On The Mechanical Properties And Fracture Modes Of SLM Ti-6Al-4V*. *Materials Science and Engineering: A* 616 (2014): p. 1-11.
- [4.3] Vandenbroucke, B. and J.P. Kruth. *Selective Laser Melting Of Biocompatible Metals For Rapid Manufacturing Of Medical Parts*. *Rapid Prototyping Journal* 13.4 (2007): p. 196-203.

- [4.4] Qiu, C., N. Adkins, and M. Attallah. *Microstructure And Tensile Properties Of Selectively Laser-Melted And Of Hiped Laser-Melted Ti–6Al–4V*. Materials Science and Engineering: A 578 (2013): p. 230-239.
- [4.5] Aboulkhair, N.. et al. *Reducing Porosity In Alsi10mg Parts Processed By Selective Laser Melting*. Additive Manufacturing 1-4 (2014): p. 77-86.
- [4.6] Leuders, S. et al. *On The Mechanical Behaviour Of Titanium Alloy Ti6Al4V Manufactured By Selective Laser Melting: Fatigue Resistance And Crack Growth Performance*. International Journal of Fatigue 48(2013): p. 300-307.
- [4.7] ASTM F2924-14, *Standard Specification for Additive Manufacturing Titanium-6 Aluminum-4 Vanadium with Powder Bed Fusion*, ASTM International, West Conshohocken, PA, 2014, www.astm.org
- [4.8] SAE AMS 4911, *Titanium Alloy, Sheet, Strip, and Plate, 6Al - 4V, Annealed*. SAE Aerospace
- [4.9] SAE AMS 2801, *Heat Treatment of Titanium Alloy Parts*, SAE Aerospace
- [4.10] S.A. David, J.M. Vitek. *Correlation between solidification parameters and weld microstructure*, International Materials Reviews, Volume 34, Number 5, (1989), p. 213-245.
- [4.11] Vrancken, Bey et al. *Heat Treatment Of Ti6al4v Produced By Selective Laser Melting: Microstructure And Mechanical Properties*. Journal of Alloys and Compounds 541 (2012): p. 177-185.
- [4.12] Knowles, C. *Residual Stress Measurement And Structural Integrity Evaluation Of SLM Ti-6Al-4V*. M. Sc. University of Cape Town, 2012: p. 167
- [4.13] Aziz, I. *MICROSTRUCTURE AND MECHANICAL PROPERTIES OF TI-6AL-4V PRODUCED BY SELECTIVE LASER SINTERING OF PREALLOYED POWDERS*. M. Eng. University of Wikato, 2010: p. 23
- [4.14] Mertens, A. et al. *Mechanical Properties Of Alloy Ti–6Al–4V And Of Stainless Steel 316L Processed By Selective Laser Melting: Influence Of Out-Of-Equilibrium Microstructures*. Powder Metallurgy 57.3 (2014): p. 184-189.
- [4.15] Xu, W. et al. *Additive Manufacturing Of Strong And Ductile Ti–6Al–4V By Selective Laser Melting Via In Situ Martensite Decomposition*. Acta Materialia 85 (2015): p. 74-84.

[4.16] Wauthle, R. et al. *Effects Of Build Orientation And Heat Treatment On The Microstructure And Mechanical Properties Of Selective Laser Melted Ti6Al4v Lattice Structures*. Additive Manufacturing 5 (2015): p. 77-84.

[4.17] J.P. Kruth, M. Badrossamay, E.Yasa, J.Deskers, L.Thijs, J.Van Humbeeck. *Part and material properties in selective laser melting of metals*, 16th International Symposium on Electromachining, ISEM XVI, 2010.

[4.18] Kobryn, P. A., and S. L. Semiatin. *Mechanical properties of laser-deposited Ti-6Al-4V.*" Solid Freeform Fabrication Proceedings. Austin, 2001.

[4.19] Rafi, H. K. et al. *Microstructures And Mechanical Properties Of Ti6Al4v Parts Fabricated By Selective Laser Melting And Electron Beam Melting*. Journal of Materials Engineering and Performance 22.12 (2013): p. 3872-3883.

[4.20] Koike, Mari et al. *Evaluation Of Titanium Alloys Fabricated Using Rapid Prototyping Technologies—Electron Beam Melting And Laser Beam Melting*. Materials 4.12 (2011): p. 1776-1792.

[4.21] Vilaro, T., C. Colin, and J. D. Bartout. *As-Fabricated And Heat-Treated Microstructures Of The Ti-6Al-4V Alloy Processed By Selective Laser Melting*. Metall and Mat Trans A 42.10 (2011): p.3190-3199.

[4.22] Murr, L.E. et al. *Microstructure And Mechanical Behavior Of Ti-6Al-4V Produced By Rapid-Layer Manufacturing, For Biomedical Applications*. Journal of the Mechanical Behavior of Biomedical Materials 2.1 (2009): p.20-32.

[4.23] Donachie, M. *Titanium: A Technical Guide*. Materials Park, Ohio: ASM International (2010): p. 59.

[4.24] Tiley, Jaimie. *MODELING OF MICROSTRUCTURE PROPERTY RELATIONSHIPS IN Ti-6Al-4V*. Ph.D. Ohio State University (2002): p.134.

Chapter 4

[4.25] Ducheyne, P., D. Kohn, and T.S. Smith. "Fatigue Properties Of Cast And Heat Treated Ti6Al4v Alloy For Anatomic Hip Prostheses". *Biomaterials* 8.3 (1987): p.223-227.

Chapter 5: Summary

As SLM is an emerging technology that has just recently been integrated into high performance manufacturing industries like aerospace, the objective of this body of work was to benchmark SLM mechanical performance against traditional modes of manufacturing. To better understand mechanical properties, an in-depth materials science approach was taken to characterize the microstructure and determine the underlying causes of mechanical behaviour.

From the results in Chapter 4, it was found that:

- (1) Through optimization of SLM machine build parameters, high density (99.6%+) specimens could be fabricated, given the proper process parameter window.
- (2) By post-processing as-built SLM samples with a stress relief heat treatment of 593°C for 2 hours, a martensitic microstructure of α' crystals was still present from the initial build process.
- (3) By post-processing as-built SLM samples with a mill anneal heat treatment of 704°C for 2 hours, the microstructure coarsened slightly, however through XRD analysis there still was no presence of β .
- (4) By post-processing as-built SLM samples with a HIP treatment of 900°C/20 ksi for 2 hours, the microstructure was completely transformed from martensitic α' to a lamellar mixture of α and β . This was confirmed through XRD, where a 3% volume fraction of β was found. Porosity was also entirely closed due to the high pressures and temperatures of the HIP process, yielding 100% dense specimens.
- (5) From visual analysis of the Euler and inverse pole figures generated by EBSD, no strong α texture was seen in either the X or Z built samples. From this, it is difficult to correlate between the mechanical properties and the crystallographic texture of the Ti- α phase from the data produced in this experiment.
- (6) Ti6Al4V SLM samples post-processed with stress relief and mill anneal heat treatments were insufficient in exceeding ductility benchmarks for both wrought and additive manufacturing standards. Extremely low elongation values in the stress relief condition are likely due to α' martensite and residual stress still being present after the treatment.

In the case of mill annealing, ductility fell short of benchmarks most likely due to remaining α' martensite and porosity.

- (7) Ti6Al4V SLM samples post-processed with HIP were sufficient in exceeding both strength and ductility benchmarks seen in wrought and additive manufacturing standards. Upon examination of the microstructure, HIP eliminated any remaining pores and transformed the as-built martensitic microstructure into a lamellar arrangement of α and β , which is most likely the cause for high final elongation values.
- (8) Anisotropy in mechanical properties was observed between the three different build orientations. Samples built in the X direction yielded the highest strengths, samples built in the Z had the lowest, while 45° had strengths between the two. Conversely, X built samples demonstrated lowered ductility when compared to Z and 45° samples. This is thought to be because of columnar grain arrangement with respect to loading direction and varying slip distances due to differences in α colony sizes for the X, 45° and Z build directions.